

Tutor/s

Dr. Joan Dosta Parras  
*Departament Enginyeria Química*

Dr. Yudania Sánchez González  
*IREC*



# Màster en Enginyeria Química

## Treball Final de Màster

**Development of a SILAR-based technology for the deposition of nanometer layers with controlled thickness for photovoltaic applications.**

**Desarrollo de una tecnología basada en el método SILAR para el depósito de capas nanométricas con espesor controlado para aplicaciones fotovoltaicas.**

Manuel Eduardo Montes Álvarez

*02/2022*



UNIVERSITAT DE  
BARCELONA

Dos campus d'excel·lència internacional

**B:KC** Barcelona  
Knowledge  
Campus

**HUB** Health Universitat  
de Barcelona  
Campus

Aquesta obra esta subjecta a la llicència de  
Reconeixement-NoComercial-SenseObraDerivada



<http://creativecommons.org/licenses/by-nc-nd/3.0/es/>



*Nunca consideres el estudio como una obligación, sino como una oportunidad para penetrar en el bello y maravilloso mundo del saber*  
Albert Einstein

En este pequeño espacio de agradecimientos, me gustaría decir grandes palabras a todas las personas que han estado apoyándome durante todo este tiempo. Primero de todo, agradecer a la Universidad de Barcelona por brindarme toda la educación recibida durante estos 6 años, con un cariño especial a todos los integrantes del Grado y del Máster en Ingeniería Química. A continuación, darle las gracias a las personas que han hecho posible este Trabajo final de Máster, que son, en primer lugar; la institución que me ha brindado la oportunidad de investigar con ellos, el Institut de Recerca en Energia de Catalunya (IREC) y el grupo de Solar Energy Materials and Systems que me acogieron con mucho cariño; a mis tutores, Yudania y Joan, por ayudarme y guiarme en todo momento; y a mi familia, por aguantarme todos los días.

# REPORT

## CONTENTS

<b>1. SUMMARY.....</b>	<b>1</b>
<b>2. INTRODUCTION.....</b>	<b>2</b>
2.1. Why photovoltaics?.....	2
2.2. Introduction to photovoltaic energy.....	3
2.3. Case study.....	8
2.3.1. Cadmium sulfide (CdS).....	9
2.3.2. Thin films.....	11
2.3.3. CBD vs SILAR.....	11
<b>3. OBJECTIVES.....</b>	<b>13</b>
<b>4. MATERIALS AND METHODS.....</b>	<b>14</b>
4.1. Materials.....	14
4.2. Methods.....	14
4.2.1. Procedure for surface morphology & optical characterization.....	14
4.2.2. Procedure for optoelectronic characterization.....	17
<b>5. RESULTS AND DISCUSSION.....</b>	<b>19</b>
5.1. First experiments.....	20
5.2. Effect of add complexing agent and pH regulator.....	21
5.2.1. Surface morphology results.....	22
5.3. Effect of nº of cycles and increasing concentrations.....	24
5.3.1. Surface morphology results.....	25
5.3.2. Optoelectronic results.....	26
5.4. Effect of cationic precursor.....	28
5.4.1. Surface morphology results.....	29
5.4.2. Optical results.....	30
5.4.3. Optoelectronic results.....	30
5.5. Final experiments.....	32
5.5.1. Surface morphology results.....	32
5.5.2. Optoelectronic results.....	33
5.5.3. Optical results.....	35
<b>6. CONCLUSIONS.....</b>	<b>36</b>
<b>7. REFERENCES AND NOTES.....</b>	<b>37</b>

## **1. SUMMARY**

The world of renewable energies, more specifically the photovoltaic energy, is a necessary technological source for humans and for the planet, but like all technological sources it is progressing. This progress it's related to a constant development of new materials and new technologies that must comply the photoelectrical requirements demanded by a photovoltaic device.

As a booming material and technology, Cadmium Sulfide (CdS) thin films and Successive Ionic Layer Adsorption and Reaction (SILAR) process will be discussed in depth and how to improve and adapt it according to the needs of the device.

Due to the fact carrying out this Final Master Project together with the help of the Energy Research Institute of Catalonia (IREC), a detailed study of improvements will be made by SILAR process. Through these experiments, different variables of SILAR will be optimized to obtain a thin layer for place it as a n-buffer and try to be able to replace the previous method used in IREC, Chemical Bath Deposition (CBD).

The main objective of this project is to optimize SILAR process for place a CdS n-buffer layer on a photovoltaic device.

So, thanks to the bibliographic search and the results of other investigations, certain conclusions have been reached that indicate that the desired objective is well on its way to being achieved.

**Keywords: Photovoltaics, Solar cell, SILAR, CBD, CdS, buffer layers**

## **2. INTRODUCTION**

### **2.1. Why photovoltaics? [1,2]**

Photovoltaic energy is a particular form of solar energy in which sunlight is converted into electricity, uses photovoltaic panels formed from an ordered succession of photovoltaic cells in which electrical energy is obtained by the photovoltaic effect. There are different ways to harness solar energy: solar thermal, which is converting sunlight into heat, or solar to fuels, which is converting sunlight into chemical energy. Among them photovoltaics has been emerged as the most widespread solar conversion technology today.

Photovoltaics is an increasingly important renewable alternative to conventional electricity generation based on fossil fuel, but compared to other technologies, it is relatively newcomer, having developed the first photovoltaic devices in 1950.

Ten years later, around the 1960s, due to the space industry's need for a grid-independent power source for satellite use, photovoltaic research and development received its first major boost. Because of their high cost, these space solar cells were unfeasible for their use in other areas.

It was not until the development of silicon transistors that solar cells became an interesting scientific variant affordable for certain niche markets.

Finally, the oil crisis of the 1970s focused the world's attention on the development of alternative energies, including photovoltaics, which promoted its research to the point where it came onto the scene as a power generation technology.

So photovoltaic energy is interesting because, together with other renewable energies, is expected to replace energy sources based on fossil fuels. Not only for environmental and climatic reasons, but also, for example, because of the risks involved. The energy consumed today is often produced in distant lands and transported at a certain risk. The Figure 1 illustrates the great risks that it has to go through to supply ourselves with energy.

Because of this, the application and advantage of photovoltaics in the field of remote power supply was quickly recognized and was the main impulse for the development of the terrestrial photovoltaic industry. It was also used for small-scale transportable applications such as calculators and watches.

The production of low-cost, high-efficiency solar cells using environmentally friendly technology is one of the greatest scientific challenges in the field of renewable energies and is the motivation of this study.





Figure 1. Example of the risks involved in energy supply

## 2.2. Introduction to photovoltaic energy

As previously mentioned, *photovoltaic energy is a particular form of solar energy in which **sunlight** is converted into electricity, uses photovoltaic panels formed from an ordered succession of **photovoltaic cells** in which electrical energy is obtained by the **photovoltaic effect**.*

For the correct understanding of this study, the concepts marked in bold will be explained:

Sunlight is the solar energy that in the form of electromagnetic waves, reaches the Earth. This effect is called solar radiation and refers to a physical vibrational phenomenon that is represented in the form of waves. The electromagnetic spectrum shown at the right (Figure 2) describes light as a wave which has a particular wavelength.

Approximately half of the solar radiation incident on the Earth's atmosphere corresponds to the frequency band of the light visible to the human eye (from 0.38  $\mu\text{m}$  to 0.78  $\mu\text{m}$ ). The rest belongs to bands that are not visible to our eyes, mainly the infrared (radiation associated with thermal processes and with wavelengths greater than 0.78  $\mu\text{m}$ ) and a small component of ultraviolet light that has wavelengths slightly smaller than the visible one (less than 0.38  $\mu\text{m}$ ). Table 1 shows this distribution. [2,3]

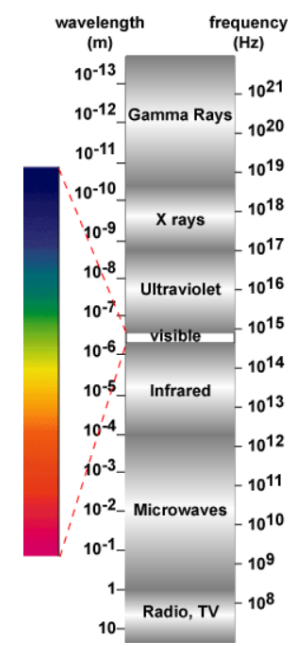


Figure 2. The electromagnetic spectrum

*Table 1. Distribution of sunlight frequency*

Band	Ultraviolet	Visible	Infrared
Wavelength [μm]	0,01-0,38	0,38-0,78	0,78-1
Energy percentage [%]	8	46	46
Radiation power [W/m <sup>2</sup> ]	109	629	629

The photovoltaic cell concept goes hand in hand with the photovoltaic effect since the operation of photovoltaic cells is based on the generation of current, thanks to the photovoltaic effect and are summarized below: [2,3,4,5]

Photovoltaic cells are mainly made up of a p-n junction, which forms the basis not only for the great majority of solar cells, but also most other electronic devices such as lasers and bipolar junction transistors. A p-n junction is a single semiconducting crystal on which one area of the material is doped with the addition of impurities, known as dopants, that can change their material conductivity. In such a way that one part is left with an of excess electrons (n-type/n-buffer), while the other area has a shortage, electron defect (p-type/p-buffer).

For example, in the case of silicon cells, atoms with one more valence electron than silicon (e.g., phosphorus) are used to produce "n-type" semiconductor material. Since phosphorus has 5 valence electrons and silicon has 4, when the two atoms bond the electrons form covalent bonds, but only 4 electrons are necessary to form the covalent bonds around the silicon atoms, so there is an extra valence electron that is free to participate in the conduction band. Complementary, atoms with one less valence electron (e.g., boron) result in "p-type" material. As in the previous case, 4 electrons are necessary to form the covalent bonds around the silicon atoms, but in this case, boron, having only 3 valence electrons does not have enough electrons to form the 4 covalent bonds surrounding the silicon atoms, this case of electron deficiency is called a hole.

So, p-n junctions are formed by joining n-type and p-type semiconductor materials. At this moment the electrons of the n-type region diffuse from the n-type region to the p-type side. Similarly, from the p-type region holes flow by diffusion to the n-type region. The holes and the electrons move to the other side of the junction, leaving behind exposed charges on dopant atom sites (positive ion cores on the n-type side and negative ion cores on the p-type side), that are fixed in the crystalline lattice and cannot be moved, this region is called the "depletion region" and is where, between the positive ion cores in the n-type material and negative ion cores in the p-type material, an electric field is formed. This mechanism is shown in Figure 3.

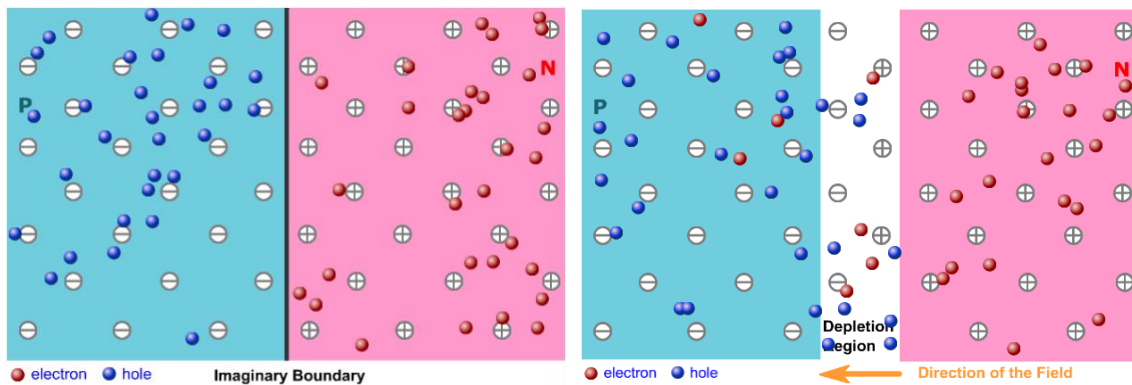


Figure 3. Example of p-n junction. Left: n-type separated from the p-type. Right: union of the two zones creating the depletion region and the electric field

The p-n junction is made up of semiconductors, the more common are shown in blue in Figure 4. A semiconductor can be either of a single element, such as Si or Ge, a compound, such as GaAs, CdS, InP or CdTe, or an alloy, such as Kesterites the most attractive as photovoltaic kesterite p-type (also called absorbers) are the  $\text{Cu}_2\text{ZnSnS}_4$  (CZTS),  $\text{Cu}_2\text{ZnSnSe}_4$  (CZTSe) y  $\text{Cu}_2\text{ZnSn}(\text{SSe})_4$  (CZTSSe). The bond structure of a semiconductor determines the material properties of a semiconductor.

		IIIA	IVA	VA	VIA	VIIA
		5	6	7	8	9
		B	C	N	O	F
		10.811	12.011	14.007	15.999	18.998
		13	14	15	16	17
		Al	Si	P	S	Cl
		26.982	28.086	30.974	32.064	35.453
IB	IIB					
29	30	31	32	33	34	35
Cu	Zn	Ga	Ge	As	Se	Br
63.54	65.37	69.72	72.59	74.922	78.96	79.909
47	48	49	50	51	52	53
Ag	Cd	In	Sn	Sb	Te	I
107.870	112.40	114.82	118.69	121.75	127.60	126.904
79	80	81	82	83	84	85
Au	Hg	Tl	Pb	Bi	Po	At
196.967	200.59	204.37	207.19	208.980	(210)	(210)

Figure 4. The more common semiconductors for p-n junctions

Semiconductors have the particularity that when illuminated with this sunlight, the electrons of the valence layer of an atom absorb the energy of the photons of light, if it is greater than the attractive forces of the nucleus, electrons are released and acquire freedom of movement in the conduction band. This space left by the electron tends to attract any other free electron. To convert this movement of electrons into electric current, it is necessary to direct the movement of the electrons, through the material to leave the cell through the N-layer surface by the low resistivity indium contacts, by creating an electric field due to the p-n junction in the material itself. The band gap represents the minimum energy that is required to excite an electron up to a state in the conduction band where it can participate in conduction. So not all photons achieve the purpose of separating electrons, this may be due to:

- Non-absorption losses due to energy loss through the material.
- No electrons are found as they pass through the semiconductor film.
- Illuminate the surface of the material and are reflected.

So, when a photovoltaic solar cell is connected, for example, to a light bulb and, at the same time, is illuminated by the sunlight, the cell work as a current generator not as a voltage generator, since the photons that arrives inside the cell and have a kinetic energy equal to or higher than the band gap, impact the material and generate electron-hole pairs. The electric field, produced by the p-n junction separates the carriers

generated in the depletion region before recombination occurs (recombination is the opposite process to electron-hole pair generation, an electron recombines with a hole and gives up the energy to produce either heat or light), when they are separated, a potential difference is created which, when in contact, makes the current flow possible, thus illuminating the bulb (Figure 5). It can be said that the current generated by an illuminated photovoltaic solar cell connected to a load is the difference between its gross production capacity and the recombination losses between electrons and photons.

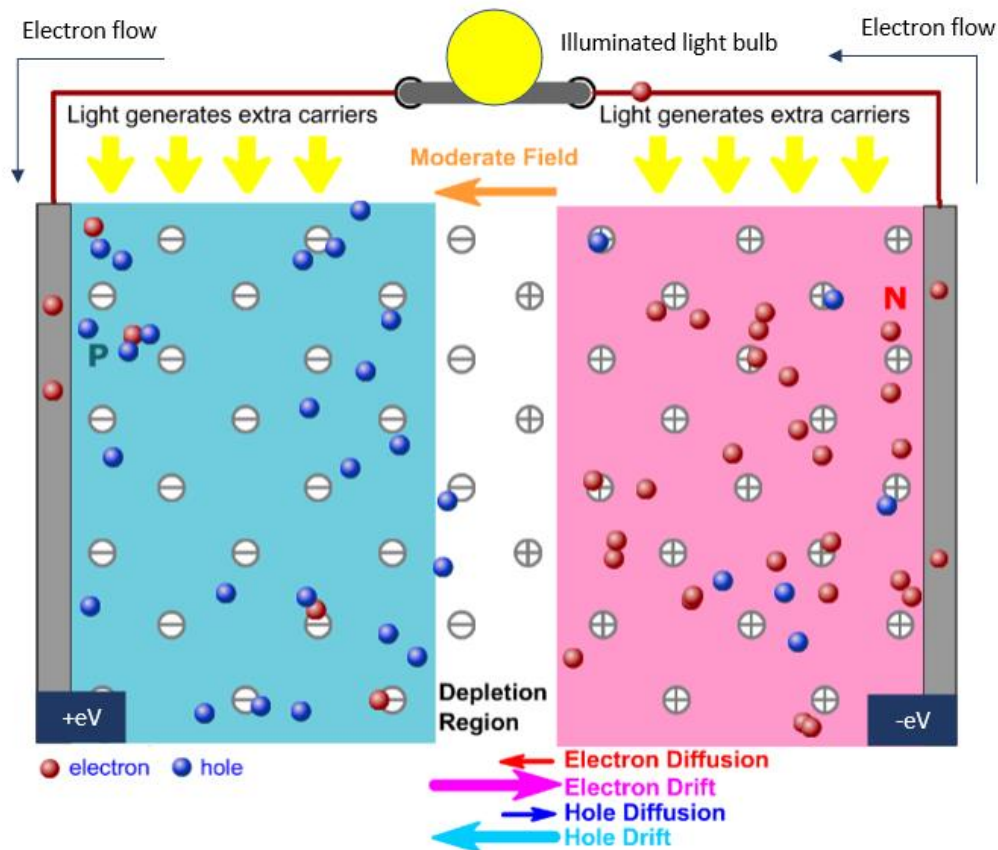


Figure 5. Operation of a photovoltaic cell

The most common and clear expression to show the behavior of the solar cell is expressing the IV curve, that represents the current it can generate at a given solar radiation, usually  $1\text{kW}/\text{m}^2$ , depending on the voltage at which the cell can work, in other words, depending on the impedance to be fed. This curve allows us to describe some characteristic points to classify, define and compare cells of different materials and/or manufacturers.

These characteristic points represented in the Figure 6 are:

- Short circuit current ( $I_{sc}/I_{cc}$ )

The short-circuit appears when the two poles of a generator come into direct electrical contact. Then, the resistance becomes minimum and, applying Ohm's law, the current becomes maximum. In the short-circuit case, the cell potential drops to almost 0 V; therefore, the carrier recombination is minimal, and the generated current is close

to the maximum possible depending on the incident solar radiation. This current value corresponds to the size of the I-V curve with the axis of the ordinates, i.e., the intensity when the voltage is 0.

- Open Circuit Voltage ( $V_{oc}/V_{oc}$ )

If the cell is in open circuit without any consumption or charge to feed, then there is no current flow to the outside of this cell. Therefore, the current is 0. When the solar cell has no load connected and is illuminated, all the generated carriers are recombined inside the cell itself. This effect causes the depletion region between the p and n material to widen and, consequently, the voltage increases to a characteristic value known as open-circuit voltage.

- Maximum power point ( $P_{mp}$ )

Observing the I-V curve, it can easily notice that each value of work voltage corresponds to an output current. If it works in direct current, then can define the electric power released by the cell as:  $P = V \cdot I$

Geometrically, each power value represents the surface of the rectangle formed by the dimensions I-V. The point of maximum power has, obviously, associated with it specific values of intensity and voltage, which we designate as:

$I_{mp}$ , intensity of the maximum power point.

$V_{mp}$ , voltage of the point of maximum power.

- Fill factor (FF)

It is a theoretical concept, useful to measure the shape of the cell curve:  $FF = P_{mp}/(I_{sc} \cdot V_{oc}) = I_{mp} \cdot V_{mp} / (I_{sc} \cdot V_{oc})$ .

- Module efficiency ( $\eta$ )

It is the ratio between the electrical power produced by the module and the incident radiation power ( $P_{in}=1kW/m^2$ ) in this module:  $\eta = V_{oc} \cdot I_{sc} \cdot FF/P_{in}$

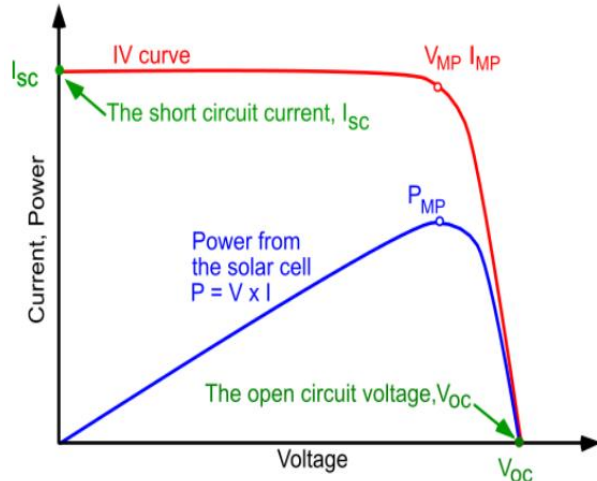


Figure 6. I-V curve

To finish with the explanation of photovoltaic cells, it is necessary to comment on their classification, since there are different types of photovoltaic cells and a multitude of ways to classify them, the classification has been chosen according to their appearance. Since the challenge in the production of photovoltaic panels is to produce high efficiency solar cells at the lowest possible cost. First generation silicon solar cells have reached a record efficiency for this material of about 25% using monocrystalline silicon, as shown in Table 2, but the cost of electrical energy produced by photovoltaic technology is so far higher than that produced by fossil fuels or nuclear energy, which has given way to the continuous study of the so-called thin film or second generation solar cells, with the aim of reducing production costs. [6]



Table 2. classification of photovoltaic cells

Technologies	Materials	Efficiency [%]
First generation	Si monocrystalline	26,3
	Si polycrystalline	21,3
Second generation	CIGS ( $\text{CuIn}_x\text{Ga}_{(1-x)}\text{Se}_2$ )	21,0
	Si amorphous	10,2
	CZTSe	9,8
Third generation	Perovskite ( $\text{CsSnI}_3$ )	19,7
	Organic cells	11,2

### 2.3. Case study

Among the types of photovoltaic cells discussed above, this study is based on the study of second generation cells, more specifically on CZTSe cells using a fabrication technology called HIT (heterojunction with intrinsic thin layer). This term refers to a technique based on the superposition of semiconductor layers of different band gap. It has been demonstrated that it improves the energy efficiency of the cells and enlarges the usable solar radiation spectrum, since each of the semiconductors is particularly sensitive to one of the bands of the electromagnetic spectrum.

An example of the cells to be worked with in this study is shown in Figure 7.

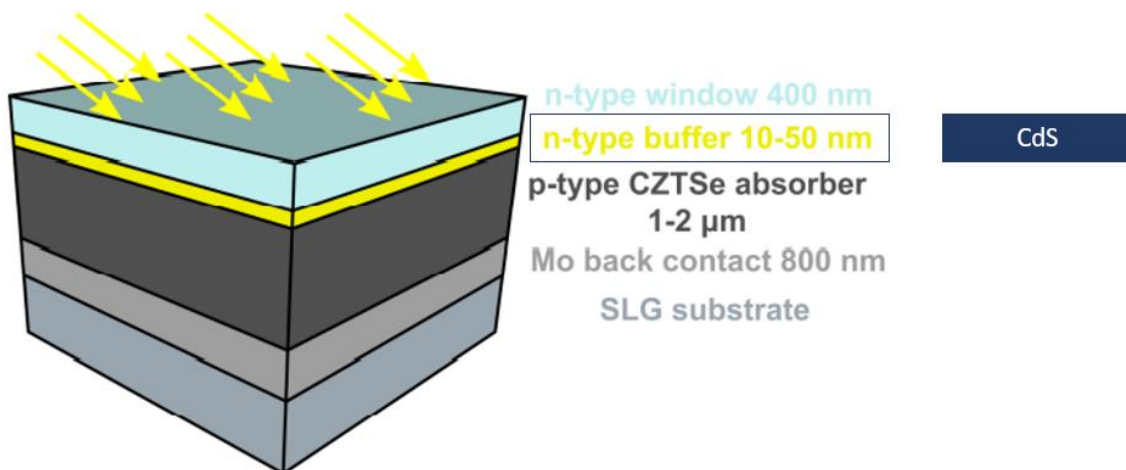


Figure 7. Example of the different parts of a photovoltaic cell

- **SLG substrate**  
Soda-lime glass substrate that supports the photovoltaic cell and is the basis for making the rest of the layers.
- **Mo back contact**  
It is the back contact of the p-type layer, constituted by molybdenum (Mo) which was deposited by sputtering on the glass substrate. The molybdenum must present adequate electrical and structural properties to allow the formation of an adequate electrical contact and consequently the correct extraction of the charge carriers photogenerated in the p-type layer.

- P-type CZTSe  
As previously mentioned, it is an alloy that acts as a p-type semiconductor. It is formed by deposition of copper (Cu), zinc (Zn) and tin (Sn) on molybdenum in sputtering and is finally converted into CZTSe by a thermal process called reactive annealing.
- N-type buffer  
In this case, it is a CdS layer processed using the SILAR method, which will be discussed in more detail later.
- N-type window (Frontal contact)  
Formed by a layer of intrinsic zinc oxide (i-ZnO) is transparent insulator that serves to isolate the holes where the n-buffer layer is not uniformly deposited. And by a layer of indium-doped tin oxide (ITO) that functions as a front contact through which the electrons will exit to the Mo back contact. Both layers are deposited by sputtering.

The production process of these photovoltaic cells is shown in Figure 8, with an inset delimiting the battery boundary of this study:

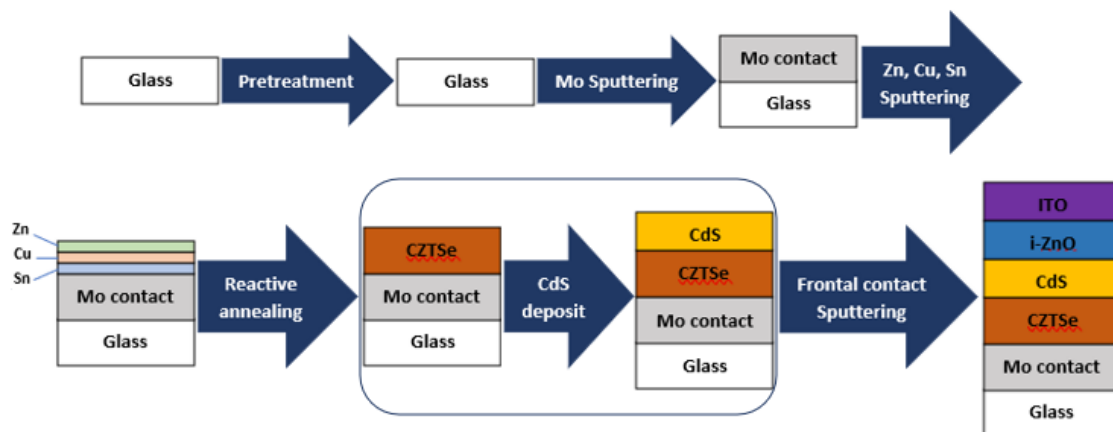


Figure 8. production process of photovoltaic cells

Therefore, this study will focus on the formation of the n-buffer *thin film* of CdS, the superposition of this layer with the p-buffer layer will be carried out using SILAR technology.

### 2.3.1. CdS

Cadmium sulfide is an important II–VI compound semiconductor, with high transparency, which is widely used in different fields (solar cells, gas sensors, photo detectors and lasers) due to its optical and electronic properties showed in Table 3.

Table 3. Principal properties of CdS

Parameters	Value
Density, $\rho$ [g/cm <sup>3</sup> ]	4.826
Dielectric constant, $\epsilon_r$ [F/m]	10
Band gap, $E_g$ [eV]	2.4

Electron affinity, $\chi$ [eV]	4.2
Electrical resistivity [W·cm]	$10^5$
Photoconductivity, $\sigma$ [ $\Omega \cdot \text{cm}$ ] <sup>-1</sup>	$1.8 \cdot 10^{-2}$
Mobility, $\mu$ [ $\text{cm}^2/(\text{V} \cdot \text{s})$ ]	0.34

The most interesting properties are direct band gap ( $E_g \sim 2.4$  eV), high electron affinity (4.2 eV) and n-type conductivity. CdS also improves the lattice heterojunction interface match and optimizes the band alignment of the devices it is used in.

To fabricate CdS thin films suitable for photovoltaic applications, they should have:

- High transparency and low thickness to avoid absorption at buffer layer.
- Large conductivity to reduce the electrical losses in the solar cells.
- Higher photoconductivity to avoid short circuiting.

In terms of its structure CdS has two crystal structure, hexagonal (wurtzite-type (W)) and cubical (zinc-blend (Z)) as shown in Figure 9. [7]

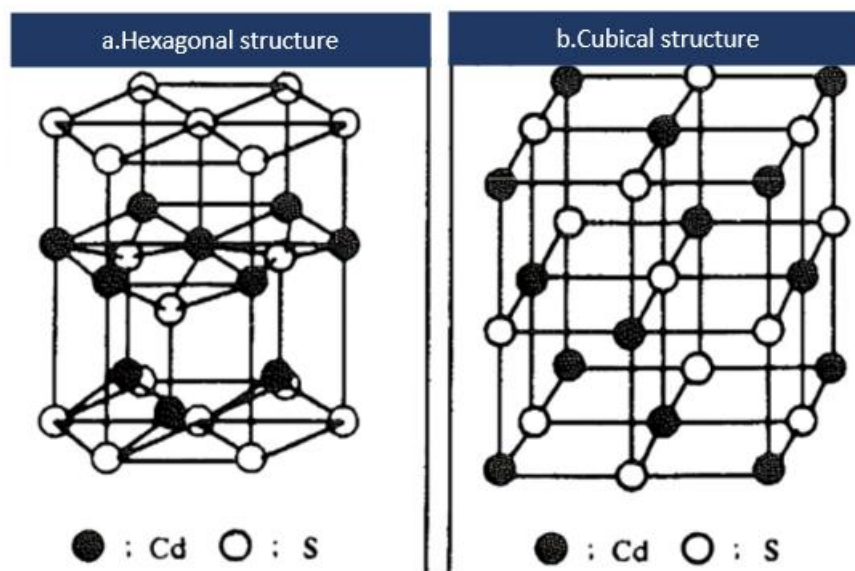


Figure 9. Structure of CdS

Each of these structures is formed mainly due to its type of growth. When the ionic product (between cadmium ( $\text{Cd}^{2+}$ ) and sulfide ( $\text{S}^{2-}$ ) ions) exceeds the solubility product of CdS ( $K_{p\text{CdS}} = 10^{-25}$ ) it precipitates either in the bulk of the solution with the formation of colloids or at the surface of the substrates leading to the formation of a film. Consequently, the film can be formed by two different mechanisms, the sedimentation of colloids called cluster-by-cluster process (obtaining cubical structure) or the direct reaction of elementary species at the surface called the ion-by-ion process (obtaining hexagonal structure). Any of these types of growth can lead to the formation of thin films but will have different properties depending on their growth mechanism. [8]



### **2.3.2. Thin films**

CdS thin films have unique physical and chemical properties compared to those of the corresponding bulk material, due to the quantum confinement effect (when electrons in a material are restricted to move in a very small region of space). Currently, thin film technology is playing an important role in improving the properties of materials.

Thin films are materials with grain sizes below 1000 nm. Due to their extremely small dimensions, a large fraction of the atoms in these materials are located at the grain boundaries, which confirms special attributes (due to surface effects, which can dominate the overall behavior of these films).

Special interest of thin films is for photovoltaic applications, optoelectronic devices, and waveguides applications among others.

Thin films can be produced in several ways. The techniques can be divided into:

- Physical methods.

The film material is moved from a source to the substrate with some kind of energy. Within the physical methods we have vacuum evaporation and sputtering, where the deposition has been transferred to the gaseous state, either by evaporation or by an impact process.

- Chemical methods

This is a chemical reaction where the precursor components reacting on or near the substrate surface. In chemical methods we have:

- Gas-phase chemical processes, such as conventional chemical vapor deposition (CVD).
- Liquid-phase chemical techniques, such as chemical bath deposition (CBD) or successive ionic layer adsorption and reaction (SILAR). [9]

### **2.3.3. CBD vs SILAR**

The deposition of CdS thin films can be performed using several methods as discussed above. Most of the techniques are either very complex and difficult to control, as well as expensive, or require stringent reaction conditions such as high temperature and pressure, and hazardous chemicals, or both. Among these techniques, CBD has been considered as one of the most common fabrication techniques for depositing a buffer layer on solar cells due to its simple deposition process, low cost and high yield, avoiding the problems discussed above. Moreover, this process can be easily controlled by variations of pH, salt concentration and temperature, thus obtaining a high-quality thin film with the desired thickness and crystallinity. But what does CBD consist of?

In general terms, CBD is essentially based on the different reactions occurring on a substrate immersed in the reaction mixture. This definition is the same as for the SILAR method (but with some differences), which gives SILAR the same characteristics as those

mentioned above for CBD. While in CBD the deposition is carried out in a single vessel, SILAR consists of 4 vessels (Figure 10) where the following process is carried out:

It is based on the formation of a thin layer on the surface of the substrate by immersing it sequentially in a saturated solution of cationic and anionic precursors, so it consists of 4 steps: [10]

- Adsorption: Of cadmium ions ( $\text{Cd}^{2+}$ ) onto the substrate
- Rising I: Of the excess adsorbed ions
- Reaction: Between cadmium ions ( $\text{Cd}^{2+}$ ) and sulfide ions ( $\text{S}^{2-}$ ) to form a CdS film
- Rising II: Of the excess adsorbed ions

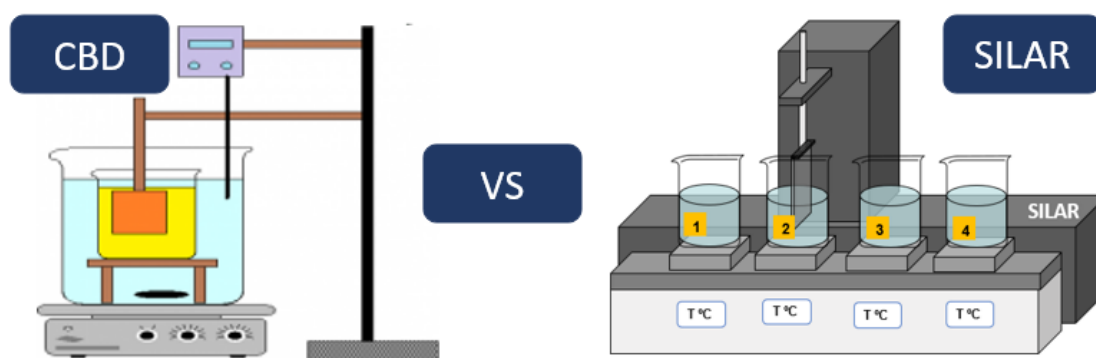


Figure 10. Mechanism comparison between CBD and SILAR

The basic mutual characteristics of the adsorption and reaction between CBD and SILAR will be described below:

- Adsorption: The collection of a substance on the surface of another substance is known as adsorption, which is the fundamental building block of CBD and SILAR method. The term adsorption can be defined as the interfacial layer between two phases of a system. In this case, there will be interaction due to the attractive force between the solution ions and the substrate surface. These forces can be cohesive forces or Van-der Waals forces or chemical forces of attraction. The atoms on the substrate surface are not surrounded by atoms or molecules of their kind on all sides, therefore, they possess unbalanced force (surface tension) and hold the substrate particles together. Factors such as pH, solution temperature and solution concentration affect the adsorption process.
- Reaction: As for the growth of the CdS film for both cases, a very controlled precipitation reaction of the desired compound on the substrate is required. Which is achieved, as discussed above, when the product of the concentrations of the ions ( $PI=[\text{Cd}^{2+}] \cdot [\text{S}^{2-}]$ ) to be precipitated in solution is only slightly higher than the value of the solubility product constant ( $K_{ps}$ ) ( $PI \geq K_{ps}$ ) of CdS. The deposition mechanism of these techniques is governed by two main processes: nucleation and particle growth. The nucleation mechanism is based on the formation of nuclei created on the surface of the solid where the film is deposited, these nuclei start from the adsorption on the surface of metal-hydroxyl ions ( $\text{Cd}(\text{OH})_2$  in this case), which are chained with other adsorbed ions

forming dispersed agglomerates. The hydroxyl anions are replaced by sulfide anions ( $S^{2-}$ ) where a first metal chalcogenide (CdS) layer is formed. The growth of the film of interest occurs on this initial film. The nucleation process can occur by association of ions on the substrate surface (ion-by-ion ion), or it can occur within the solution (cluster-by-cluster). If nucleation occurs within the solution, large agglomerates are formed, which can lead to precipitation of the material in the reaction vessel instead of on the substrate, which decreases the efficiency of the process. Even if these agglomerates adhere to the substrate surface, the deposit obtained is not homogeneous and does not have good adhesion. In contrast, ion-by-ion growth shows good adhesion, homogeneous growth and better efficiencies, making it the desired growth for photovoltaic applications. The nucleation mechanism can be controlled to be predominantly ion-by-ion by low reaction rates, which can be achieved by using dilute solutions (on the order of  $10^{-3}$  mol/L) of the ions to be precipitated, a high concentration of the complexing agent (one or two orders higher, if this component is added), low temperatures and vigorous agitation in the system. [11]

The basic differences between CBD and SILAR will be described below:

By taking place in 4 different containers allows SILAR, compared to CBD, to be more:

- Safe and environmentally friendly: less intermediates are generated by not directly contacting the precursor solutions.
- Easy to control: Since it is controlled by cycles.

On the other hand, using the SILAR method requires more expensive equipment and more variables to control which makes it slightly more complex since the characteristics of thin layer depends on its deposition conditions (substrate type, temperature of the precursor solutions, numbers of dipping cycles, the dipping time and concentration and pH of precursor solutions), but if optimized correctly the benefits are more noticeable in the long run than the disadvantages. [12]

Therefore, one of the purposes of this study is to optimize these SILAR deposition conditions to obtain CdS thin films comparable/better than the CBD method. The objectives are detailed below.

### **3. OBJECTIVES**

The main objective of this project is to optimize SILAR process for place a CdS n-buffer layer on a photovoltaic device.

In order to reach this objective, it is necessary to achieve small specific objectives such as:

- Which is the best pretreatment for the substrates?
- Which is the best cationic precursor?

- Which is the best anionic precursor?
- Which are the best SILAR variables?
- Which is the best post-treatment?









#### 4. MATERIALS AND METHODS [13,14]

The materials and methods used are summarized in this section.

##### 4.1. MATERIALS

Table 4 shows the different reactants used throughout this study.

Table 4. Principal reactants

Reagent	Chemical formula	Quantity [g]	Pictogram CLP	CAS NO.	Laboratory
Cadmium acetate dihydrate (99.999%)	$\text{Cd}(\text{CH}_3\text{COO})_2 \cdot 2\text{H}_2\text{O}$	25		57430404	Alfa Aesar
Cadmium chloride	$\text{CdCl}_2$	50		10108-64-2	Sigma Aldrich
Cadmium iodide	$\text{CdI}_2$	50		7790-80-9	Sigma Aldrich
Cadmium nitrate tetrahydrate	$\text{Cd}(\text{NO}_3)_2 \cdot 4\text{H}_2\text{O}$	30		10022-68-1	Sigma Aldrich
Sodium sulfide	$\text{Na}_2\text{S}$	50		1313-82-2	Sigma Aldrich
Thiourea	$\text{H}_2\text{NCSNH}_2$	100		62-56-6	Sigma Aldrich
Sodium citrate	$\text{Na}_3\text{C}_6\text{H}_5\text{O}_7$	10		68-04-2	Sigma Aldrich
Ammonium hydroxide	$\text{NH}_4\text{OH}$	1 L*		1336-21-6	Sigma Aldrich

##### 4.2. METHODS

The preparation of the coatings for their characterization was carried out by means of two series of procedures, one procedure for their surface morphology and optical characterization and another procedure for their optoelectronic characterization, as detailed below. All the substrates for the different coatings have dimensions of 50x25x1mm

##### 4.2.1. Procedure for surface morphology and optical characterization

Figure 11 shows the procedure followed to perform the surface morphology and optical characterization, for which a Fluorine-doped Tin Oxide (FTO) substrate is coated:

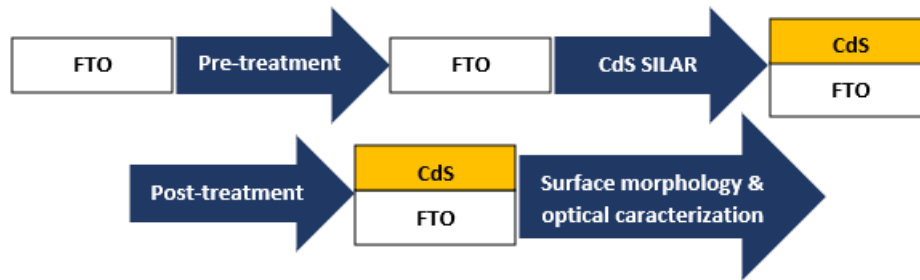


Figure 11. Production process for surface morphology and optical characterization

The steps followed are:

- Pretreatment

The pretreatment established by IREC for the different substrates is: Substrate washing with glass soap + dissolution in water of hydrochloric acid (HCl) (10%) for 10min + deionized water + isopropanol (CH<sub>3</sub>CH(OH)CH<sub>3</sub>) and drying with argon (Ar).

- Coating by the SILAR method

The coating conditions used to obtain the final coatings presented in this study were proposed based on the experience and work obtained in previous studies with these materials. The main SILAR working conditions recorded by the bibliography are shown in Table 5:

Table 5. Principal SILAR working conditions

Cationic precursor	Anionic precursor	Precursor conc. [M]	Nº Cycles	Temperature [°C]	Dipping time (Ad, R1, Re, R2) [s]
CdCl <sub>2</sub> , Cd(CH <sub>3</sub> COO) <sub>2</sub> · 2H <sub>2</sub> O, CdI <sub>2</sub> Cd(NO <sub>3</sub> ) <sub>2</sub> · 4H <sub>2</sub> O	Na <sub>2</sub> S, H <sub>2</sub> NCSNH <sub>2</sub>	0,0025-0,5	20-80	30-90	10-60

A broader view of these experiments is shown in the following results and discussion section. To obtain the coatings, a Silar Coating System with Magnetic Stirrer & Ultrasonic Bath model: HO-TH-03C located in the facilities of the Solar Materials and Systems Group - IREC was used (Figure 12).



Figure 12. Example of SILAR mechanism

- Post-treatment

Post-treatment was carried out by thermal annealing in a rapid thermal annealing (RTA) furnace which is a method to improve material properties. These treatments are performed after deposition of the n-buffer layer without having completed the front contact. The rapid annealing process allows samples to be subjected to high temperatures, capable of inducing structural changes, for very short periods of time. The RTA treatments were carried out in a model RTA AS-ONE furnace from Annealsys Company (Figure 13). Initially, two argon (Ar) cleanings are performed to avoid any contaminant and a heating ramp of 20°C/s was used to achieve a temperature of 200°C for 10 min.



Figure 13. Example of rapid thermal annealing (RTA) furnace

To determine the properties of the coatings, they were characterized by:

- Scanning Electron Microscopy (SEM)

The characterization of the coatings was carried out using a scanning electron microscope (Figure 14) belonging to IREC. The main objective of the observation is to compare and identify the properties of the coatings obtained, allowing a qualitative evaluation. The scanning electron microscope (SEM) uses the information sent by the secondary and backscattered electrons of a solid sample to construct an image. For the morphological study of the n-buffer layers, ZEISS FESEM equipment was used. The usual operating conditions were detector InLens, voltage at 2-5 kV and a work distance around 2mm. The magnifications used varied between x10000 and x100000 magnification.



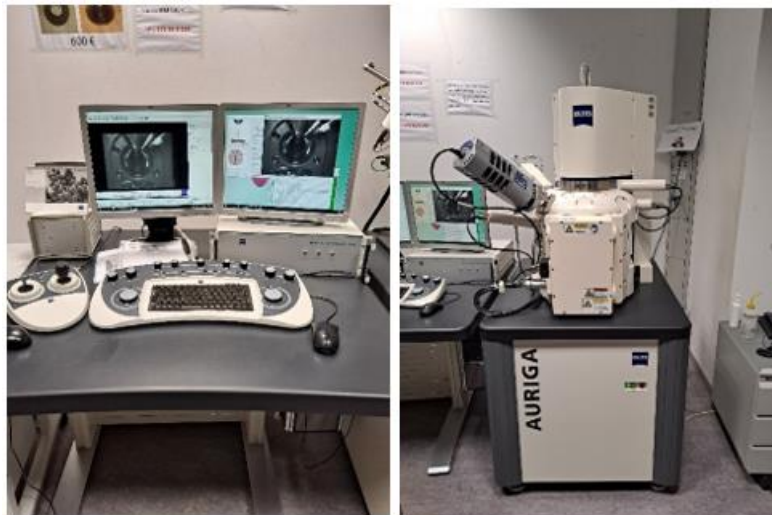


*Figure 14. Example of SEM*

- Ultraviolet-Visible transmittance spectroscopy (UV-visible)

Optical transmittance refers to the amount of light that passes through a body at a given wavelength. When a beam of light strikes a translucent body, some of that light is reflected, some is absorbed, and the rest is transmitted through the body. Transmittance (T) is thus a measure of the attenuation of light. Thus, when an isolated molecule absorbs a photon, the energy of one or more valence electrons increases. Ultraviolet-Visible transmittance spectroscopy has many applications in quantitative analysis within chemical analysis. The optical response of buffer layers with respect to transmittance and absorbance properties in the UV-VIS wavelength range is very important to achieve optically optimized buffer layers. For the characterization of the buffer layers used in the present study, a Perkin Elmer Lambda double beam UV-Vis spectrophotometer was used, allowing us to know the transmittance of the films (Figure 15).



*Figure 15. Example of ultraviolet-visible transmittance spectroscopy*

#### **4.2.2. Procedure for optoelectronic characterization**

Figure 16 shows the procedure followed to perform the optoelectronic characterization, for which a photovoltaic cell is treated as follows:

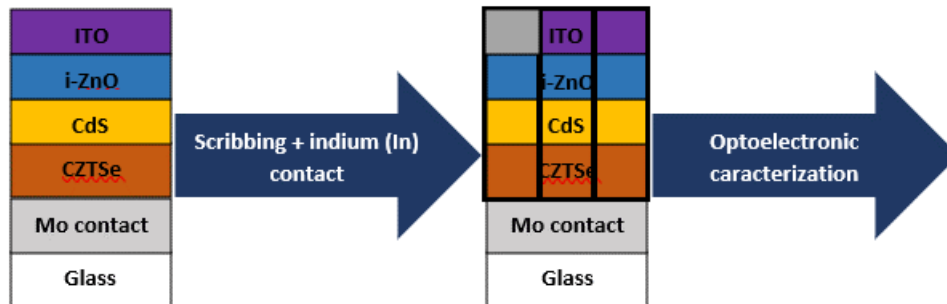


Figure 16. Production process for optoelectronic characterization

- Scribing and indium contact

There are two processes to prepare the photovoltaic cell for optoelectronic characterization. Scribing consists of segmenting the cell into equal parts (3x3mm) so that each sub-cell has the same area when measuring (Figure 17). On the other hand, the indium contact is a layer through which the electrons exit due to its low resistivity.



Figure 17. Example of a scribing machine

- Voltage-Current Characteristic Curve (SOLAR)

The fundamental characterization of a photovoltaic device is the measurement of the current-voltage curves (I-V curves). To obtain the data that characterize the electrical response of the solar cell, the measurement is carried out under standard lighting conditions (at 25°C, an irradiation of 1 kW/m<sup>2</sup> and with an AM 1.5 filter). An ABET TECHNOLOGIES solar simulator of the sun 3000 series was used for this purpose. An image of this equipment is shown in Figure 18. This equipment is connected to a data acquisition software, through which the measurement is programmed. After the measurement, the I-V curve is obtained and the most important parameters of the device are automatically evaluated: Short Circuit Current Density (I<sub>sc</sub>), Open Circuit Voltage (V<sub>oc</sub>), Fill Factor (FF) and Efficiency (η).

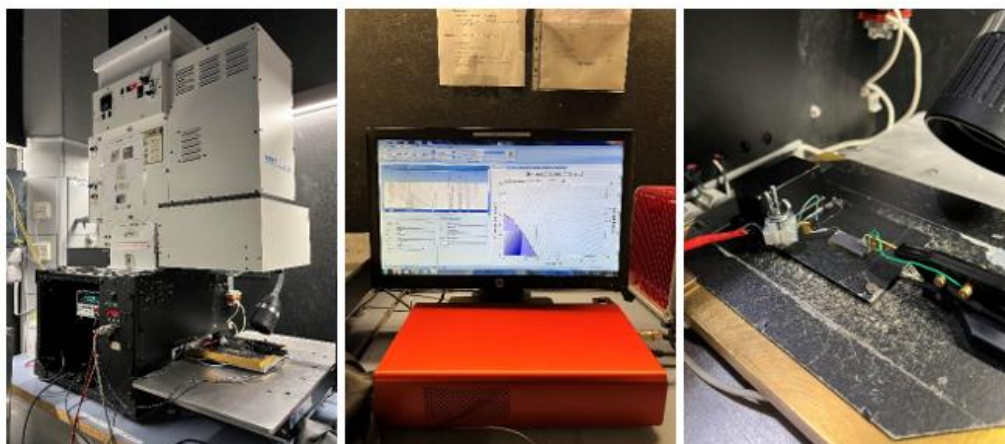
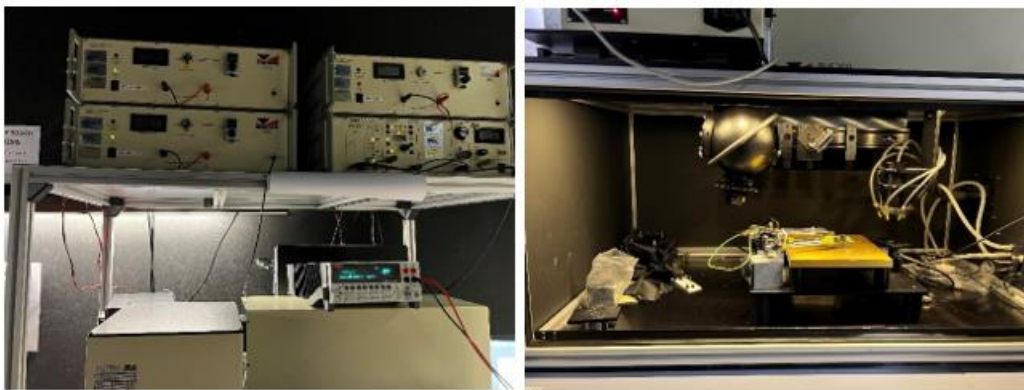


Figure 18. Example of SOLAR



- Spectral response (EQE)

The spectral response is measured in the same configuration as the I-V curve measurements, except that the incandescent lamp is replaced by a monochromatic light source with which the intensity is calibrated. The BENTH PVE300 system from BENTHAM was used to determine the spectral response of the devices, with which the external quantum efficiency (EQE) can be determined, which is the ratio between the number of photons adsorbed by the solar cell and the number of photons of a given energy incident on the solar cell; in the case of CdS, it shows absorption in the range of 350 to 650nm. This system uses a xenon/quartz halogen light source, giving coverage in a spectral range of 350-2500 nm. Figure 19 shows this measurement system.



*Figure 19. Example of spectral response mechanism*

## 5. RESULTS AND DISCUSSION

The most relevant experiments and the results obtained are presented below.

In order to carry out this study, the following variables have been set:

- Pretreatment

The pretreatment established by IREC for the different substrates is:

Substrate washing with glass soap + dissolution in water of hydrochloric acid (HCl) (10%) for 10min + deionized water + isopropanol ( $\text{CH}_3\text{CH}(\text{OH})\text{CH}_3$ ) and drying with argon (Ar).

- Post-treatment

The post-treatment performed for the different substrates is:

Annealing 10min at 423K since it shows highest electrical conductivity and highest thermoluminescence efficiency for CdS films [15].







Factors considered:

- To avoid the sulfide deficiencies detected by several authors, due to the migration of loosely bound cadmium ions ( $\text{Cd}^{2+}$ ) from the substrate to the anionic solution, it was determined that the anionic solution should be changed every 30-40 cycles [16].

- The temperature of the baths is maintained at 80°C, since this temperature is reported as the optimum for the better uniformity of CdS films [17].

As shown in the previous section on materials and methods, IREC has the following precursors for the formation of CdS represented at the Table 6.

Table 6. Principal precursors

Reagent	Chemical formula	Quantity [g]	Pictogram CLP	CAS NO.	Laboratory
Cadmium acetate dihydrate (99.999%)	$\text{Cd}(\text{CH}_3\text{COO})_2 \cdot 2\text{H}_2\text{O}$	25		57430404	Alfa Aesar
Cadmium chloride	$\text{CdCl}_2$	50		10108-64-2	Sigma Aldrich
Cadmium iodide	$\text{CdI}_2$	50		7790-80-9	Sigma Aldrich
Cadmium nitrate tetrahydrate	$\text{Cd}(\text{NO}_3)_2 \cdot 4\text{H}_2\text{O}$	30		10022-68-1	Sigma Aldrich
Sodium sulfide	$\text{Na}_2\text{S}$	50		1313-82-2	Sigma Aldrich
Thiourea	$\text{H}_2\text{NCSNH}_2$	100		62-56-6	Sigma Aldrich

### 5.1. First experiments

For the first experiments, the bibliography used by the different authors was followed as a reference. Among the different articles, those using the most interesting pair of precursors reported in the first SILAR research by Nicolau et al. [18] were used,  $\text{CdCl}_2$  and  $\text{Na}_2\text{S}$ , as shown in Table 7.

Table 7. First experiments

Experiment	Cationic precursor	Anionic precursor	Cationic conc. [M]	Anionic conc. [M]	Nº Cycles	Temperature [°C]	Dipping time (Ad, R1, Re, R2) [s]	Bibliography
Z1	$\text{CdCl}_2$	$\text{Na}_2\text{S}$	0,005	0,0025	40	80	15, 10, 15, 10	
Z2	$\text{CdCl}_2$	$\text{Na}_2\text{S}$	0,005	0,005	40	80	15, 10, 15, 10	[18]
Z3	$\text{CdCl}_2$	$\text{Na}_2\text{S}$	0,005	0,010	40	80	15, 10, 15, 10	
Z4	$\text{CdCl}_2$	$\text{Na}_2\text{S}$	0,2	0,1	40	80	15, 10, 15, 10	
Z5	$\text{CdCl}_2$	$\text{Na}_2\text{S}$	0,1	0,1	40	80	15, 10, 15, 10	[19]
Z6	$\text{CdCl}_2$	$\text{Na}_2\text{S}$	0,1	0,2	40	80	15, 10, 15, 10	

<b>z7</b>	CdCl <sub>2</sub>	Na <sub>2</sub> S	0,025	0,05	40	80	15, 10, 15, 10	[20]
<b>z8</b>	CdCl <sub>2</sub>	Na <sub>2</sub> S	0,025	0,1	40	80	15, 10, 15, 10	

Due to the non-coating of the first experiments, mainly because of a poor adsorption of the cationic precursor as shown in Figure 20, it was decided to vary the precursors, following other experiments, add complexing agents that introduce a supplementary activated kinetic step of decomplexing, thus increasing the surface relaxation time that promotes a regular growth [18], and work at a high levels of pH, to promote hydrolysis and increase the negative charge of the substrate surface, since, the hydrolysis of cadmium ions improves adsorption [21].



Figure 20. Example of unsatisfactory coatings

## 5.2. Effect of add complexing agent and pH regulator

Therefore, sodium citrate (Na<sub>3</sub>C<sub>6</sub>H<sub>5</sub>O<sub>7</sub>) was added as a complexing agent to the cationic precursor and some drops of ammonium hydroxide (NH<sub>4</sub>OH) were also added to both precursors, to work at a constant pH of 10. After applying these changes, the following results shown in Table 8 were obtained.

Table 8. Experiments of the effect of the addition of a complexing agent and a pH regulator.

Experiment	Cationic precursor	Anionic precursor	Cationic conc. [M]	Anionic conc. [M]	Nº Cycles	Temperature [°C]	Dipping time (Ad, R1, Re, R2) [s]	Bibliography
<b>01</b>	Cd(CH <sub>3</sub> COO) <sub>2</sub> · 2H <sub>2</sub> O + 0.5M Na <sub>3</sub> C <sub>6</sub> H <sub>5</sub> O <sub>7</sub> (10ml) + 2ml of NH <sub>4</sub> OH (pH=10)	Na <sub>2</sub> S + 1ml of NH <sub>4</sub> OH (pH=10)	0,0125	0,05	60	80	20, 20, 20, 20	[22]
<b>02</b>	Cd(CH <sub>3</sub> COO) <sub>2</sub> · 2H <sub>2</sub> O + 0.5M Na <sub>3</sub> C <sub>6</sub> H <sub>5</sub> O <sub>7</sub> (10ml) + 2ml of NH <sub>4</sub> OH (pH=10)	Na <sub>2</sub> S + 1ml of NH <sub>4</sub> OH (pH=10)	0,025	0,1	60	80	20, 20, 20, 20	

<b>03</b>	Cd(CH <sub>3</sub> COO) <sub>2</sub> · 2H <sub>2</sub> O + 0.5M Na <sub>3</sub> C <sub>6</sub> H <sub>5</sub> O <sub>7</sub> (10ml) + 2ml of NH <sub>4</sub> OH (pH=10)	Na <sub>2</sub> S + 1ml of NH <sub>4</sub> OH (pH=10)	0,05	0,2	60	80	20, 20, 20, 20
<b>04</b>	CdCl <sub>2</sub> + 0.5M Na <sub>3</sub> C <sub>6</sub> H <sub>5</sub> O <sub>7</sub> (10ml) + 2ml of NH <sub>4</sub> OH (pH=10)	H <sub>2</sub> NCSNH <sub>2</sub> + 1ml of NH <sub>4</sub> OH (pH=10)	0,01	0,05	40	80	15, 15, 15, 15
<b>05</b>	CdCl <sub>2</sub> + 0.5M Na <sub>3</sub> C <sub>6</sub> H <sub>5</sub> O <sub>7</sub> (10ml) + 2ml of NH <sub>4</sub> OH (pH=10)	Na <sub>2</sub> S + 1ml of NH <sub>4</sub> OH (pH=10)	0,01	0,05	40	80	15, 15, 15, 15

[17]

These experiments were properly coated.



Figure 21. Example of satisfactory coatings

### 5.2.1. Surface morphology results

Once good coatings were obtained as shown in Figure 21, they were characterized by SEM to observe the surface morphology and see how the coating was arranged.



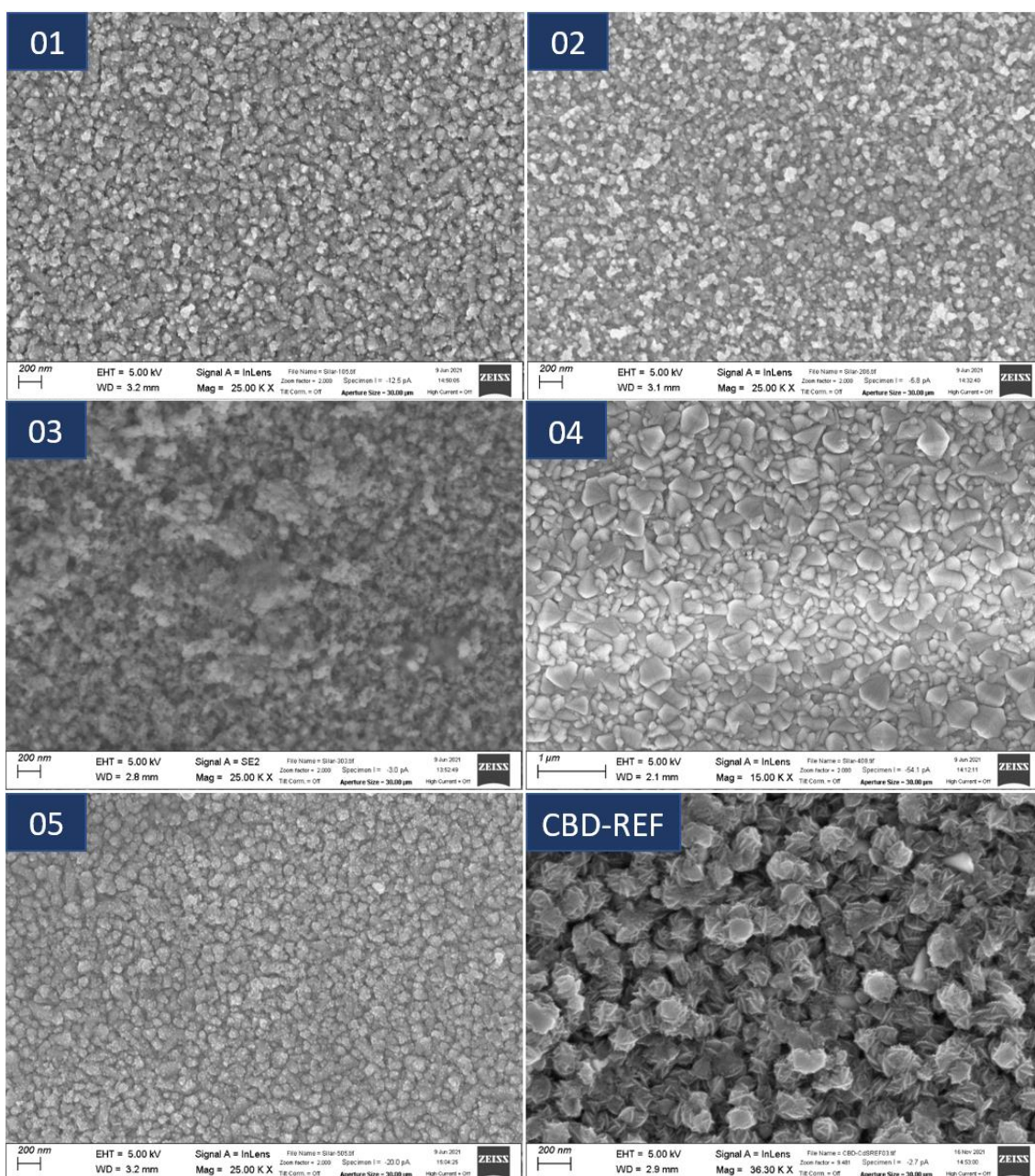


Figure 22. SEM results of the experiments of the effect of the addition of a complexing agent and a pH regulator and CBD (CBD-REF)

It was observed at the Figure 22, that the most promising coating was experiment 04 as it presents a more uniform coating. This is because ion-by-ion growth was formed against the rest of the experiments which are formed by the cluster-by-cluster growth. Ion-by-ion presents strong adhesion and homogeneous films and cluster by cluster growing from a colloidal dispersion that is known to be loose and powdery [23].

This result is also in agreement with the literature, which reports that the optimum molar ratio of cationic and anionic precursors for obtaining good quality CdS films is 1:5. It has been found that stoichiometry is achieved when the S/Cd ratio in the starting solution is 5:1. When the stoichiometry is close, CdS films have lower resistivity

values suitable for photovoltaic applications. So, these ratios will be maintained throughout the different experiments [24].

Figure 23 shows a comparison, on FTO, of an uncoated substrate vs. the experiment 04 to see their difference.

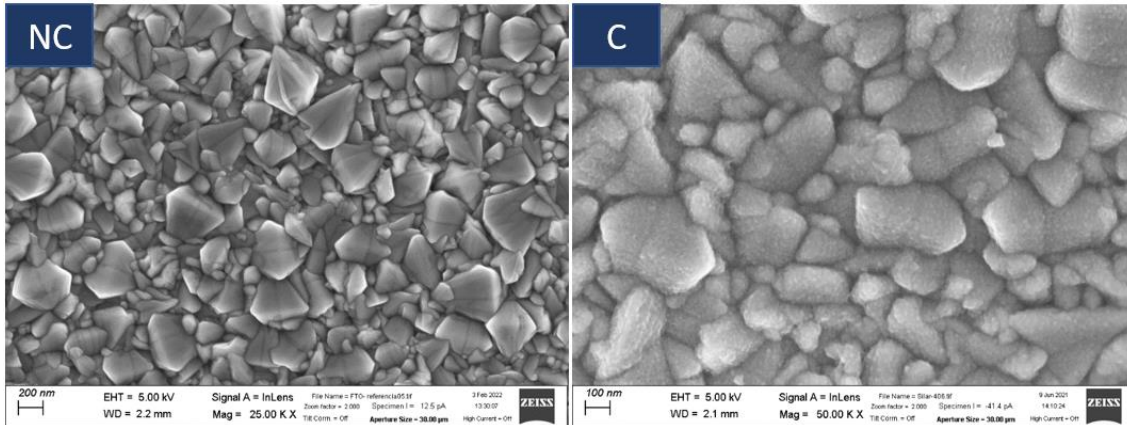
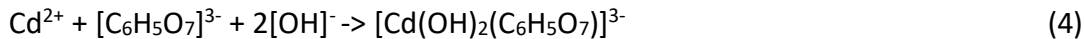


Figure 23. SEM results of comparison on FTO, of an uncoated substrate (NC) and the experiment 04 (C)

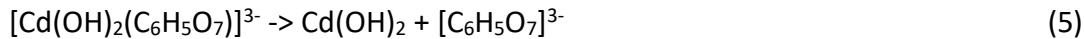
It was determined that the formation of films with Na<sub>2</sub>S leads to the formation of colloids at the liquid so that a cluster-by-cluster growth is formed instead of the ion-by-ion growth.

Therefore, the use of Na<sub>3</sub>C<sub>6</sub>H<sub>5</sub>O<sub>7</sub>, NH<sub>4</sub>OH and H<sub>2</sub>NCSNH<sub>2</sub> was determined necessary to achieve films with controlled ion-by-ion growth. The reaction and mechanism on which it is based is [25,26]:

**Adsorption:** CdCl<sub>2</sub>, Na<sub>3</sub>C<sub>6</sub>H<sub>5</sub>O<sub>7</sub> and NH<sub>4</sub>OH dissolves in water.

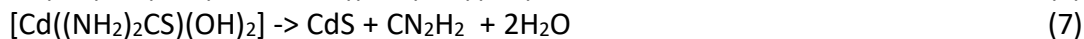
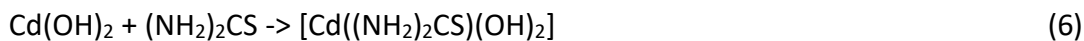


The cadmium component dissociates, and Cd(OH)<sub>2</sub> is adsorbed on the substrate.



**Rinsed I:** Counter ions (Cl<sup>-</sup>) and Cd(OH)<sub>2</sub> poorly adhered are rinsed

**Reaction:** Thiourea is adsorbed and reacts:



Reaction of adsorbed cadmium ions with sulfide ions:



**Rinsed II:** Counter ions are rinsed.

### 5.3. Effect of n° of cycles and increasing concentrations

Thus, following the line of experiment 04, experiments 06 and 07 were done. Experiment 06 corresponds to the same as experiment 04 but varying the number of

cycles, and experiment 07 was done following the same procedure as experiment 06 but changing the concentrations of the precursors maintaining same molar ratio of 1:5, increasing them to try to reduce the number of cycles and make the process faster. Table 9 shows the experiments carried out.

Table 9. Experiments of the effect of n° of cycles and increasing concentrations

Experiment	Cationic precursor	Anionic precursor	Cationic conc. [M]	Anionic conc. [M]	N° Cycles	Temperature [°C]	Dipping time (Ad, R1, Re, R2) [s]
06	CdCl <sub>2</sub> + 0.5M Na <sub>3</sub> C <sub>6</sub> H <sub>5</sub> O <sub>7</sub> (10ml) + 2ml of NH <sub>4</sub> OH (pH=10)	H <sub>2</sub> NCSNH <sub>2</sub> + 1ml of NH <sub>4</sub> OH (pH=10)	0,01	0,05	20/30/40/50	80	15, 15, 15, 15
07	CdCl <sub>2</sub> + 0.5M Na <sub>3</sub> C <sub>6</sub> H <sub>5</sub> O <sub>7</sub> (10ml) + 2ml of NH <sub>4</sub> OH (pH=10)	H <sub>2</sub> NCSNH <sub>2</sub> + 1ml of NH <sub>4</sub> OH (pH=10)	0,1	0,5	20	80	15, 15, 15, 15

### 5.3.1. Surface morphology results

These experiments were characterized by SEM in Figure 24 to verify the good coating reported in experiment 04.



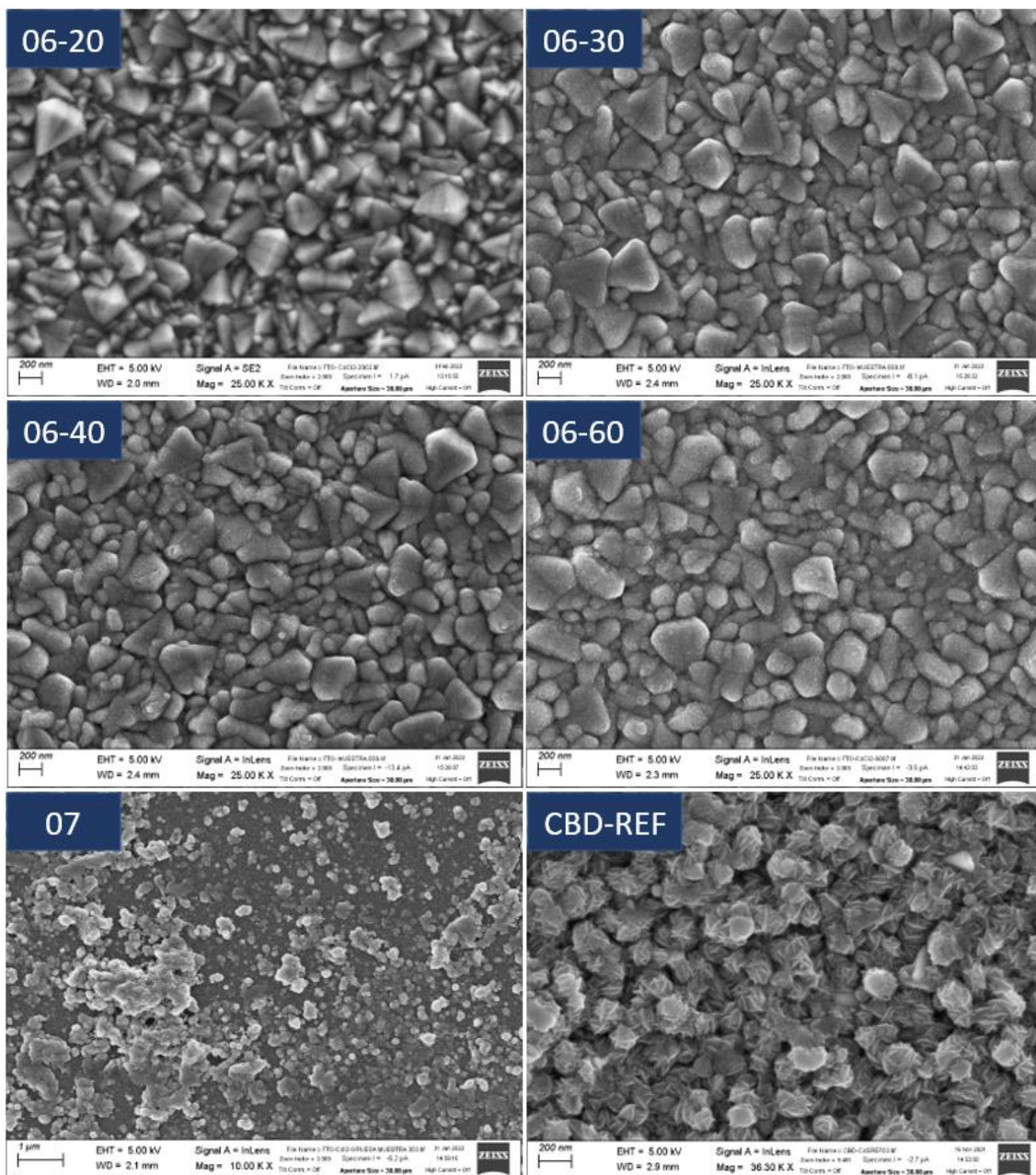


Figure 24. SEM results of the experiments of the effect of  $n^{\circ}$  of cycles and increasing concentrations: (06-20) corresponds to experiment 06 for 20 cycles, (06-30) corresponds to experiment 06 for 30 cycles, (06-40) corresponds to experiment 06 for 40 cycles, (06-60) corresponds to experiment 06 for 50 cycles, (07) corresponds to experiment 07 and (CBD-REF) corresponds to CBD

An increase in roughness is observed with increasing number of cycles for experiment 06, related to an increase in thickness. But all coatings apparently present the same type of growth (ion-by-ion).

As for experiment 07, like experiment 03, is formed by cluster-by-cluster growth which, due to colloid formation for the use of high concentrations, results in a heterogeneous, powdery film.

### 5.3.2. Optoelectronic results



Due to the good coatings of the experiment 06, the optoelectronic properties were measured in the SOLAR, from which the results in Figure 25 were obtained.

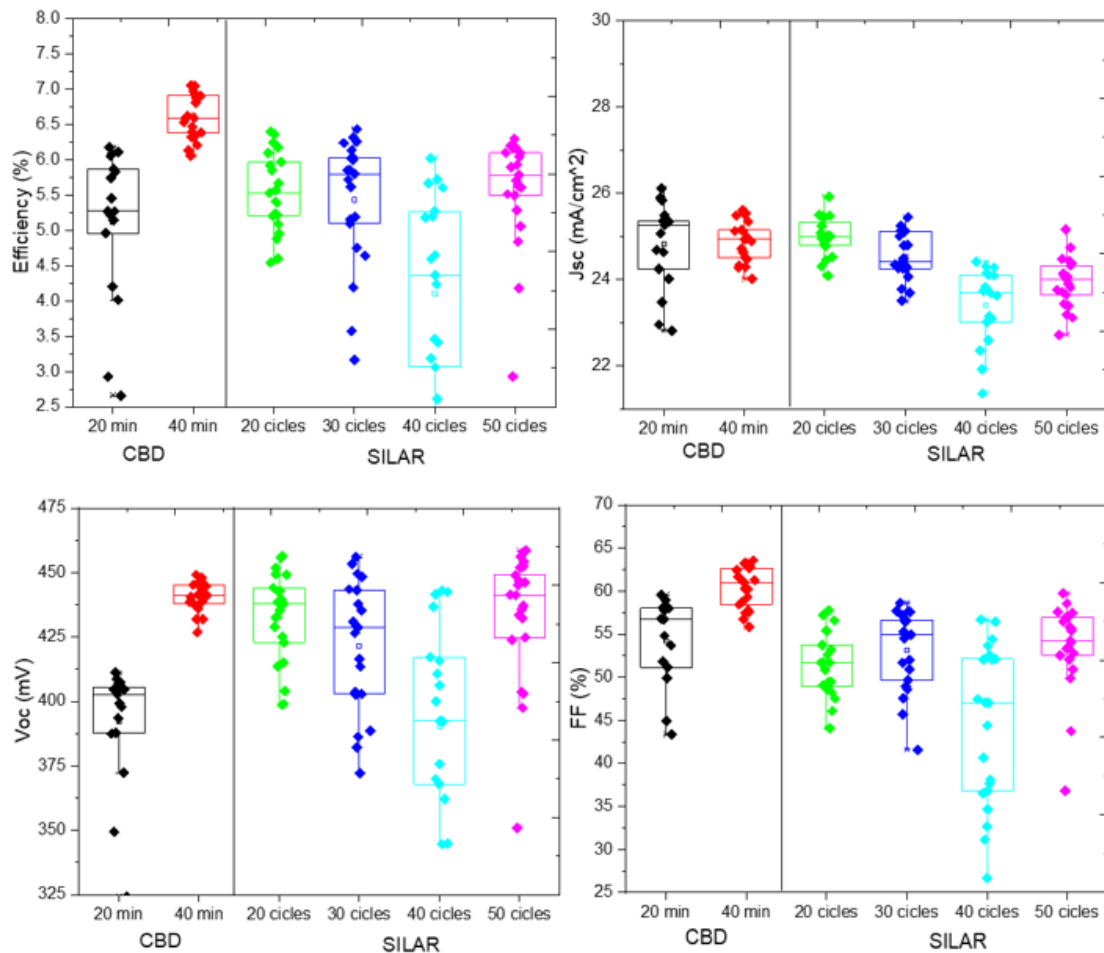


Figure 25. SOLAR results of the experiments of the effect of the addition of a complexing agent and a pH regulator and CBD

It is observed that the efficiency of CBD at 40min is the highest, but SILAR presents similar and superior results in some aspects as in the case of Voc.

Due to damage in the absorber, the experiments will be repeated for 40 and 50 cycles, but a slight tendency is observed that the higher the number of cycles, the higher the efficiency. This data agrees with the bibliography since the quality of the crystal increases [27].

Following this trend hypothesis, a cross-section study was performed in the SEM to determine the number of cycles necessary to reach the required thickness limit for the n-buffer layer, about 50 nm, which was 60 cycles as shown in Figure 26. Therefore, experiment 06 will be repeated, at 40 and 60 (instead of 50) cycles.

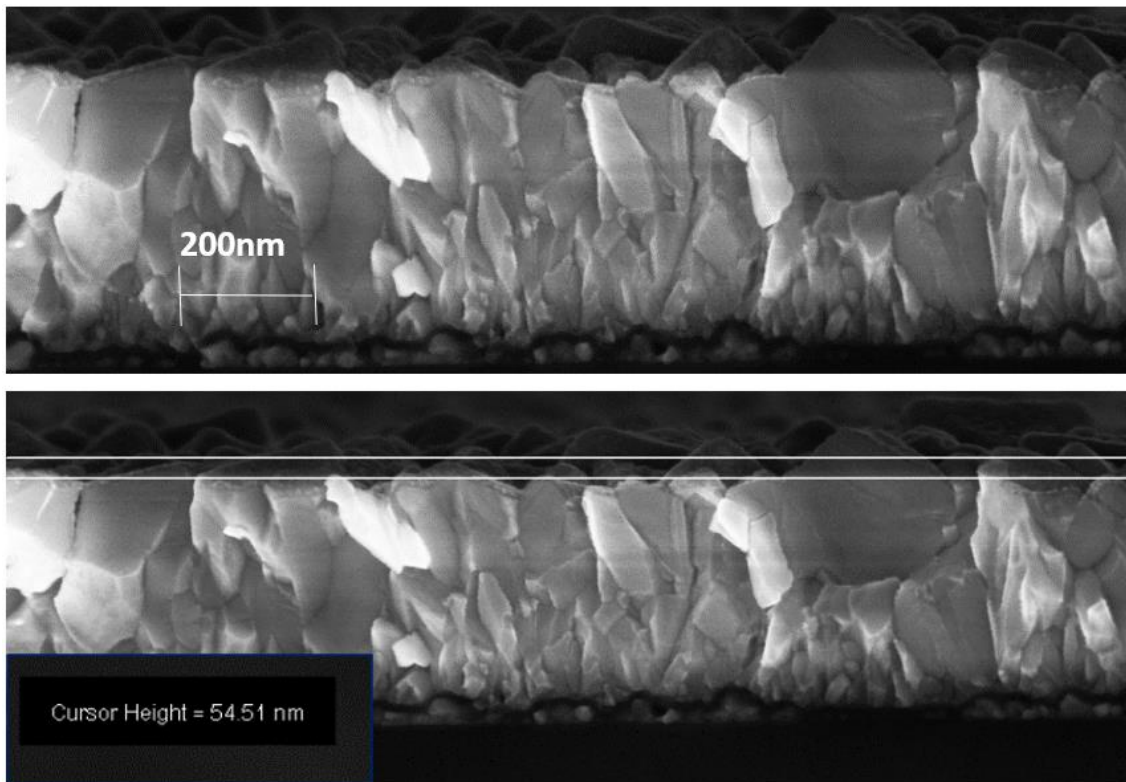


Figure 26. SEM results of the cross-section

#### 5.4. Effect of cationic precursor

On the other hand, it was decided to study the behavior of the films with different cationic precursors by fixing the rest of the variants like the experiment 06 at the two most promising cycles to obtain the coatings 40 and 60 cycles as shown in Table 10.

Table 10. Experiments of the effect of cationic precursor

Experiment	Cationic precursor	Anionic precursor	Cationic conc. [M]	Anionic conc. [M]	Nº Cycles	Temperature [°C]	Dipping time (Ad, R1, Re, R2) [s]
A1	CdI <sub>2</sub> + 0.5M Na <sub>3</sub> C <sub>6</sub> H <sub>5</sub> O <sub>7</sub> (10ml) + 2ml of NH <sub>4</sub> OH (pH=10)	H <sub>2</sub> NCSNH <sub>2</sub> + 1ml of NH <sub>4</sub> OH (pH=10)	0,01	0,05	40	80	15, 15, 15, 15
A2	CdI <sub>2</sub> + 0.5M Na <sub>3</sub> C <sub>6</sub> H <sub>5</sub> O <sub>7</sub> (10ml) + 2ml of NH <sub>4</sub> OH (pH=10)	H <sub>2</sub> NCSNH <sub>2</sub> + 1ml of NH <sub>4</sub> OH (pH=10)	0,01	0,05	60	80	15, 15, 15, 15
B1	Cd(NO <sub>3</sub> ) <sub>2</sub> · 4H <sub>2</sub> O + 0.5M Na <sub>3</sub> C <sub>6</sub> H <sub>5</sub> O <sub>7</sub> (10ml) + 2ml of	H <sub>2</sub> NCSNH <sub>2</sub> + 1ml of NH <sub>4</sub> OH (pH=10)	0,01	0,05	40	80	15, 15, 15, 15

	NH <sub>4</sub> OH (pH=10)						
<b>B2</b>	Cd(NO <sub>3</sub> ) <sub>2</sub> · 4H <sub>2</sub> O + 0.5M Na <sub>3</sub> C <sub>6</sub> H <sub>5</sub> O <sub>7</sub> (10ml) + 2ml of NH <sub>4</sub> OH (pH=10)	H <sub>2</sub> NCSNH <sub>2</sub> + 1ml of NH <sub>4</sub> OH (pH=10)	0,01	0,05	60	80	15, 15, 15, 15
<b>C1</b>	Cd(CH <sub>3</sub> COO) <sub>2</sub> · 2H <sub>2</sub> O + 0.5M Na <sub>3</sub> C <sub>6</sub> H <sub>5</sub> O <sub>7</sub> (10ml) + 2ml of NH <sub>4</sub> OH (pH=10)	H <sub>2</sub> NCSNH <sub>2</sub> + 1ml of NH <sub>4</sub> OH (pH=10)	0,01	0,05	40	80	15, 15, 15, 15
<b>C2</b>	Cd(CH <sub>3</sub> COO) <sub>2</sub> · 2H <sub>2</sub> O + 0.5M Na <sub>3</sub> C <sub>6</sub> H <sub>5</sub> O <sub>7</sub> (10ml) + 2ml of NH <sub>4</sub> OH (pH=10)	H <sub>2</sub> NCSNH <sub>2</sub> + 1ml of NH <sub>4</sub> OH (pH=10)	0,01	0,05	60	80	15, 15, 15, 15

#### 5.4.1. Surface morphology results

The morphological results shown by the SEM exhibit similarities between the films as illustrated in Figure 27.

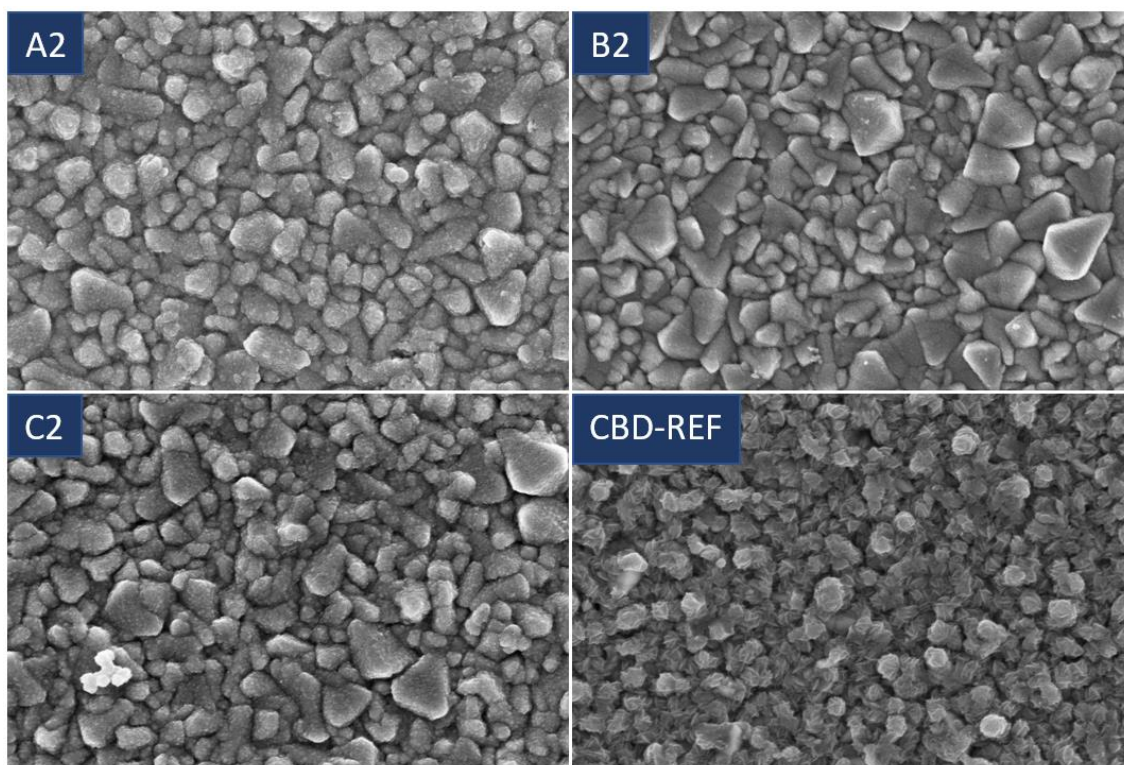


Figure 27. SEM results of the effect of cationic precursor and CBD (CDS-REF)

Despite the similarities in the films, it seems that the most promising film is B2, which corresponds to  $\text{Cd}(\text{NO}_3)_2$ , the same cationic precursor as for CBD.

#### 5.4.2. Optical results

Because there are no differences large enough to determine which is better, as an additional test, UV-visible spectroscopy was performed to determine their optical properties. The results are shown in Figure 28.

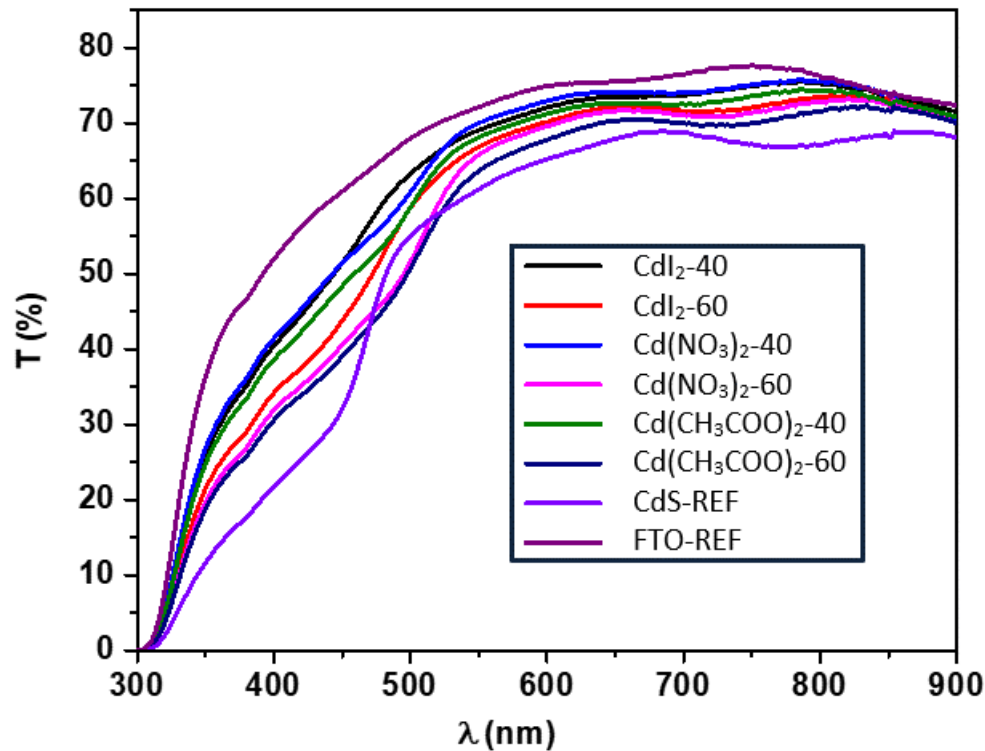


Figure 28. UV-visible results of the effect of cationic precursor

The optical transmission spectra of the CdS films were measured in the range of 300-900 nm. The sharp absorption edge of the spectra indicates the good crystallinity of the films. The average transmittance in the visible range is found to be in the range of 65-80% [24]. It is observed that coatings made with SILAR show higher transmittance values.

Cadmium nitrate is finally selected as the most promising precursor among these. Moreover, the values of optical transmittance and optical band gap decrease with increasing number of immersion cycles as reported in the literature [27].

#### 5.4.3. Optoelectronic results

As for its optoelectronic properties, the results were analyzed in SOLAR and EQE was performed. To finalize this study of the cationic precursor, the optoelectronic results were compared between SILAR with this precursor and CBD in the SOLAR, this comparison is shown in Figure 29, the comparison is represented by the blue colors

(representing SILAR at 40 and 60 cycles) and green (representing CBD at 40min), the rest are other experiments that were measured at the same time that should not be considered.

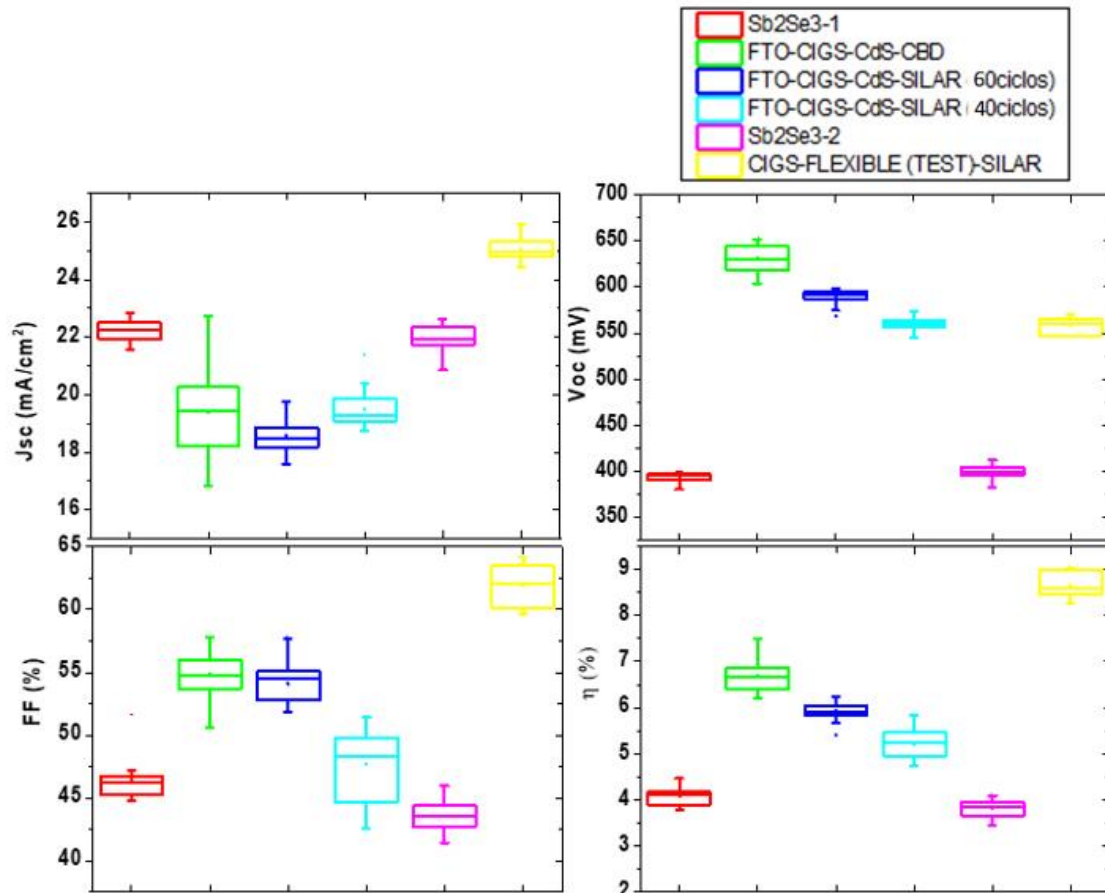


Figure 29. SOLAR results of the effect of cationic precursor

The optoelectrical results shown in the SOLAR reflect a similar result to the first experiments, where the CBD shows a higher yield than the SILAR and the SILAR shows a higher yield at a higher number of cycles. In this case the CBD Voc is considerably higher than in SILAR.

The EQE between CBD and SILAR at 60 cycles (which presented a higher yield) was also performed, this is reflected in Figure 30.

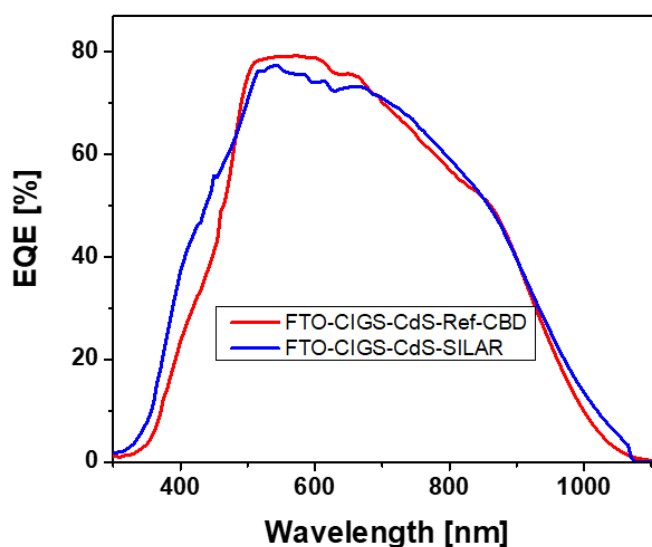


Figure 30. EQE results of the effect of cationic precursor

It can be observe a notable improvement of the EQE in the region of short wavelengths for the buffer grown by the SILAR method, which favors the reduction of current losses associated with the absorption of photons in the buffer layer.

### 5.5. Final experiment

Finally,  $\text{CdCl}_2$  and  $\text{Cd}(\text{NO}_3)_2$ , corresponding to experiments 06 and B2 by SILAR vs. CBD of 40min were compared as shown in Table 11:

Table 11. Final experiments

Experi ment	Cationic precursor	Anionic precursor	Cationic conc. [M]	Anionic conc. [M]	Nº Cycles	Tempera ture [°C]	Dipping time (Ad, R1, Re, R2) [s]
06	$\text{CdCl}_2 + 0.5\text{M}$ $\text{Na}_3\text{C}_6\text{H}_5\text{O}_7$ (10ml) + 2ml of $\text{NH}_4\text{OH}$ (pH=10)	$\text{H}_2\text{NCSNH}_2$ + 1ml of $\text{NH}_4\text{OH}$ (pH=10)	0,01	0,05	20/40/60	80	15, 15, 15, 15
B2	$\text{Cd}(\text{NO}_3)_2 \cdot$ $4\text{H}_2\text{O} + 0.5\text{M}$ $\text{Na}_3\text{C}_6\text{H}_5\text{O}_7$ (10ml) + 2ml of $\text{NH}_4\text{OH}$ (pH=10)	$\text{H}_2\text{NCSNH}_2$ + 1ml of $\text{NH}_4\text{OH}$ (pH=10)	0,01	0,05	60	80	15, 15, 15, 15

#### 5.5.1. Surface morphology results

Figure 31 shows the morphology of the different samples already shown in this section, in which the expected growth can be observed.



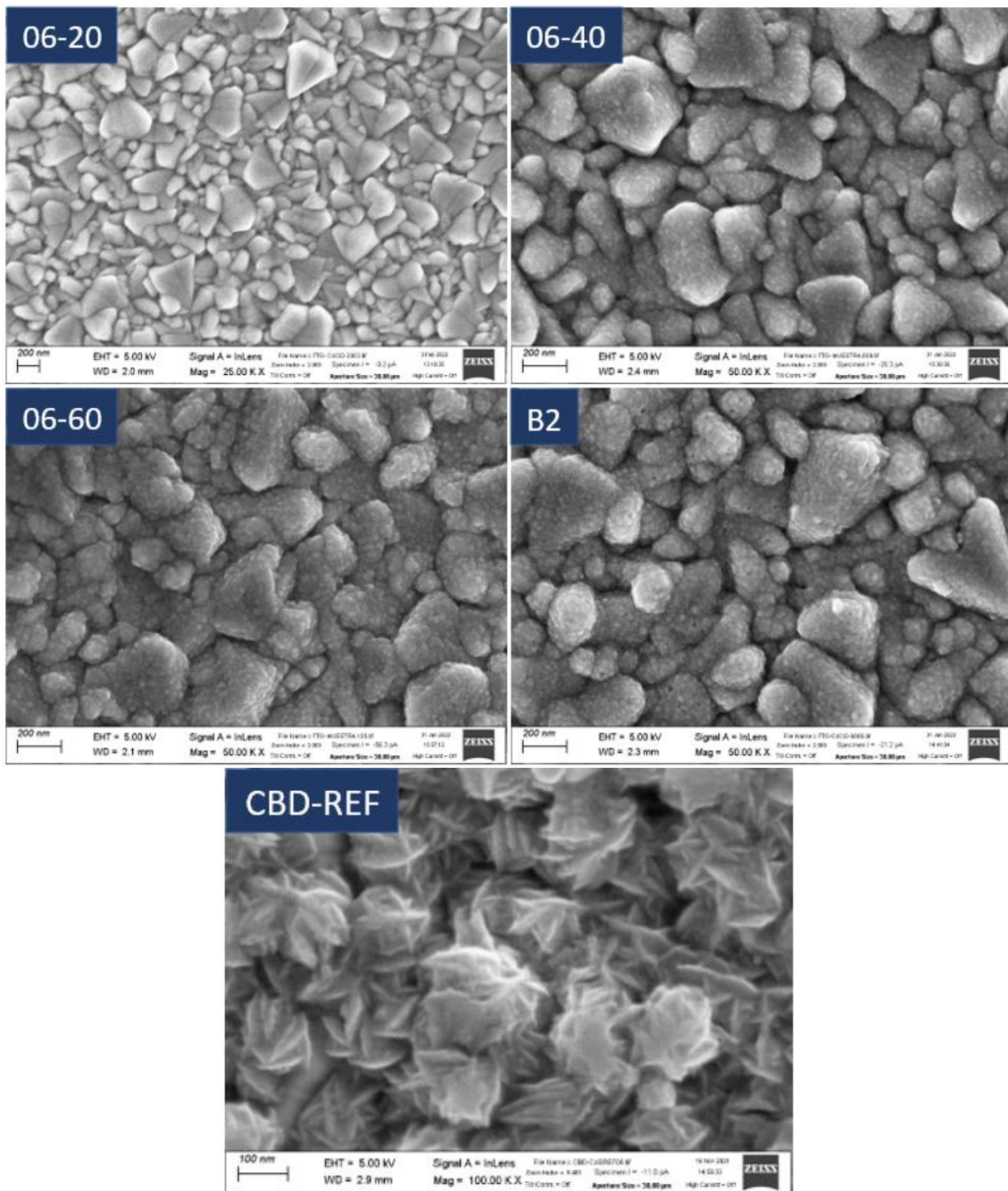


Figure 31. SEM results of the final experiments cadmium chloride at 20 (06-20), 40 (06-40) and 60 (06-60) cycles; cadmium nitrate at 60 cycles (B2) and CBD (CBD-REF).

### 5.5.2. Optoelectronic results

The optoelectronic results, for SOLAR and EQE, are shown in Figure 32 and 33 respectively.

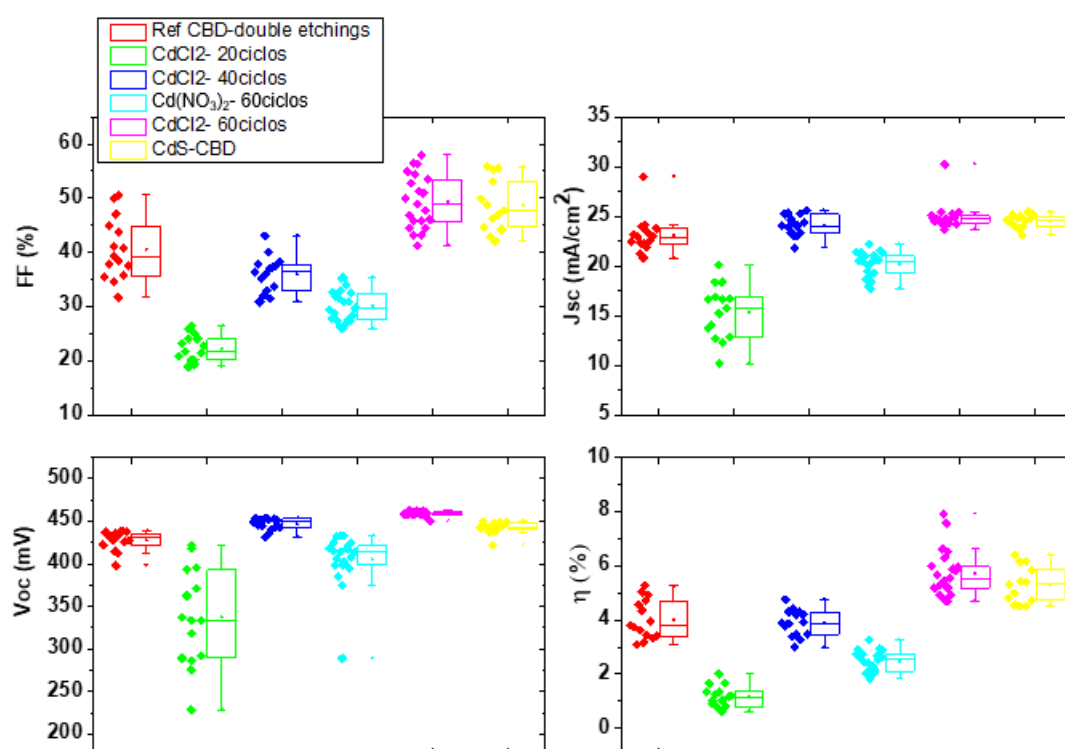


Figure 32. SOLAR results of the final experiments

It is observed that the cationic precursor, CdCl<sub>2</sub>, experiment (06) for 60 cycles, presents a higher efficiency than CBD. Comparison parameters between CBD and SILAR are shown in Table 12.

Table 12. I-V parameters of CBD and SILAR

Deposition method	J <sub>sc</sub> [mA/cm <sup>2</sup> ]	V <sub>oc</sub> [mV]	FF [%]	η [%]
CBD	25,48	449,54	55,84	6,39
SILAR	30,31	450,29	58,04	7,92

All parameters are better for SILAR (60 cycles) compared to CBD.

As for nitrate, it presents less efficiency than chloride, and according to Borges et al. [8] cadmium chloride presents the highest growth rate among the different cadmium precursors. Therefore, it would be necessary to study the thickness reached by nitrate.

As previously mentioned, an increase in the number of cycles is associated with a greater thickness and higher efficiencies since it is found that the crystal quality gradually increases with the number of immersion cycles.

On the other hand, it was decided to compare this SILAR 60 cycles with CBD by means of an EQE. (The red curve of the EQE must be ignored).



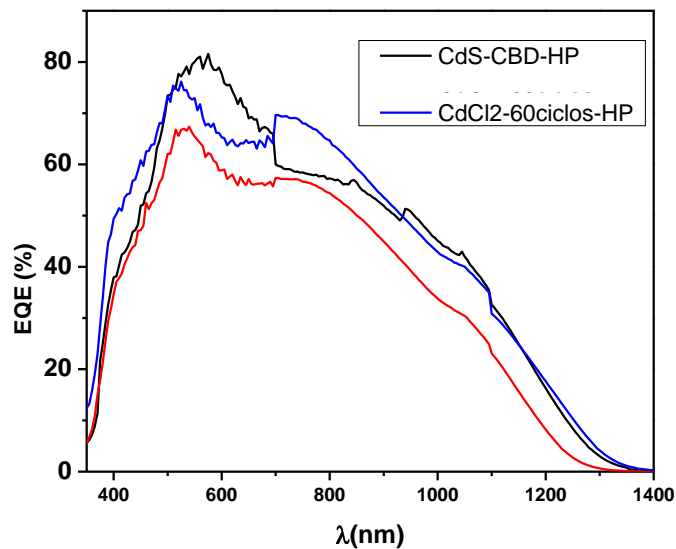


Figure 33. EQE results of the final experiments

The EQE of the devices obtained with the CdS and SILAR is shown, where the influence of the thickness of the buffer layer in the response of the cell in the region of short wavelengths, being CdCl<sub>2</sub> and using 60 cycles the most promising for increasing current in the solar devices under study because of its improvement of the EQE in the region of short wavelengths.

### 5.5.3. Optical results

The optical results performed by UV-visible are shown in Figure 34, only the experiments referring to CdCl<sub>2</sub>, for all the cycles, have been measured since it presents the highest efficiency.

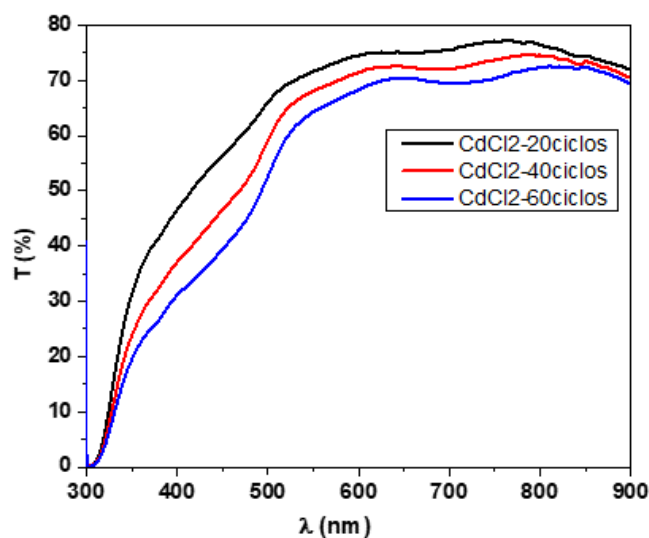


Figure 34. UV-visible results of the final experiments

All of them have good transmittance and the lower the number of cycles, the lower the thickness and therefore the easier it is for light to pass through.

## **6. CONCLUSIONS**

CdS thin films with good morphological, optical and optoelectronic properties have been obtained by SILAR method. The use of  $\text{Na}_3\text{C}_6\text{H}_5\text{O}_7$  as complexing agent and  $\text{NH}_4\text{OH}$  as pH regulator has been determined necessary for a correct adsorption of the cationic precursor. As an anionic precursor, thiourea ( $\text{H}_2\text{NCSNH}_2$ ) shows ion-by-ion growth (under the conditions proposed in this study) while sodium sulfate ( $\text{Na}_2\text{S}$ ) shows cluster-by-cluster growth. It is found that increasing the number of cycles leads to an increase in efficiency since it is found that the crystal quality gradually increases with the number of immersion cycles. The CdS thin films grown with SILAR show remarkable improvement of the transmittance and EQE in the region of short wavelengths, which favors the reduction of current losses associated with the absorption of photons in the buffer layer. Finally, the SOLAR results allow us to conclude that the development of the SILAR technology can give higher efficiencies than CBD in the production of CdS thin films.

Further research will follow in this line to try to reduce the process time and try to make the SILAR process a viable process for industrial applications.

## 7. REFERENCES AND NOTES

- [1] MITopencourseware. Massachusetts Institute of Technology. <https://ocw.mit.edu/courses/mechanical-engineering/2-627-fundamentals-of-photovoltaics-fall-2013/lecture-videos-slides/2011-lecture-1-introduction/> (accessed Aug 23, 2021)
- [2] PVEducation. PVEducation. <https://www.pveducation.org> (accessed Oct 11, 2021)
- [3] Institut català d'energia (ICAEN). [http://icaen.gencat.cat/web/.content/10\\_ICAEN/17\\_publicacions\\_informes/04\\_coleccio\\_QuadernPractic/quadern\\_practic/arxiu/20201201\\_QP4\\_web.pdf](http://icaen.gencat.cat/web/.content/10_ICAEN/17_publicacions_informes/04_coleccio_QuadernPractic/quadern_practic/arxiu/20201201_QP4_web.pdf)
- [4] Electrons and holes. Shockley W: 1950.
- [5] Shockley W. The Theory of p-n Junctions in Semiconductors and p-n Junction Transistors.
- [6] Green MA, Emery K, Hishikawa Y, Warta W, Dunlop ED, Levi DH, et al. Solar cell efficiency tables (version 49). *Progress in Photovoltaics: Research and Applications*. 2017 Jan 1;25(1):3–13.
- [7] Najm AS, Chelvanathan P, Tiong SK, Ferdaous MT, Shahahmadi SA, Yusoff Y, et al. Numerical insights into the influence of electrical properties of n-CdS buffer layer on the performance of SLG/Mo/p-absorber/n-CdS/n-ZnO/Ag configured thin film photovoltaic devices. *Coatings*. 2021 Jan 1;11(1):1–17.
- [8] Ortega-Borges R, Lincot D. Mechanism of Chemical Bath Deposition of Cadmium Sulfide Thin Films in the Ammonia-Thiourea System: In Situ Kinetic Study and Modelization. *Journal of The Electrochemical Society*. 1993 Dec 1;140(12):3464–73.
- [9] Soonmin H, Bilal Tahir M, Das SN, Das MR. PREPARATION OF THIN FILMS BY SILAR AND SPIN COATING METHOD. *Eurasian Journal of Analytical Chemistry*.
- [10] Pathan HM, Lokhande CD. Deposition of metal chalcogenide thin films by successive ionic layer adsorption and reaction (SILAR) method. Vol. 27, *Bull. Mater. Sci*. 2004.
- [11] Cortes A, Gómez H, Marotti RE, Riveros G, Dalchiele EA. Grain size dependence of the bandgap in chemical bath deposited CdS thin films. In: *Solar Energy Materials and Solar Cells*. 2004. p. 21–34.
- [12] Ashok A, Regmi G, Romero-Núñez A, Solis-López M, Velumani S, Castaneda H. Comparative studies of CdS thin films by chemical bath deposition techniques as a buffer layer for solar cell applications. *Journal of Materials Science: Materials in Electronics*. 2020 May 1;31(10):7499–518.
- [13] Adria Limeres Requena. CARACTERIZACIÓN DE CÉLULAS SOLARES DE CONTACTOS POSTERIORES IBC [Internet]. Available from: <https://upcommons.upc.edu/bitstream/handle/2117/105477/TFGfin.pdf?sequence=1>
- [14] Sánchez González Y. Síntesis química de capas buffer para nuevas tecnologías de calcogenuros con aplicaciones fotovoltaicas [Internet]. Available from: [www.tdx.cat](http://www.tdx.cat)
- [15] Metin H, Erat S, Emen FM, Kafadar V, Yazici AN, Ari M, et al. The thermoluminescence properties of CdS films under nitrogen atmosphere. *Journal of Luminescence*. 2010 Aug;130(8):1531–8.
- [16] Banu NN, Ravichandran K. Analysis of sulphur deficiency defect prevalent in SILAR-CdS films. *Journal of Materials Science: Materials in Electronics*. 2017 Aug 1;28(16):11584–90.

- [17] Ravichandran K, Philominathan P. Comparative study on structural and optical properties of CdS films fabricated by three different low-cost techniques. *Applied Surface Science*. 2009 Mar 15;255(11):5736–41.
- [18] Nicolau YF. SOLUTION DEPOSITION OF THIN SOLID COMPOUND FILMS BY A SUCCESSIVE IONIC-LAYER ADSORPTION AND REACTION PROCESS \*. Vol. 22, *Applications of Surface Science*. 1985.
- [19] Valkonen MP, Lindroos S, Kanninen T, Leskela M, Tapper U, Kauppinen E. Thin multilayer CdSrZnS films grown by SILAR technique. Vol. 120, *Applied Surface Science*. 1997.
- [20] Sankapal BR, Mane RS, Lokhande CD. Deposition of CdS thin films by the successive ionic layer adsorption and reaction (SILAR) method. 2000.
- [21] Raquel Garza Hernandez. DEPÓSITO DE PELÍCULAS DELGADAS DE Cu<sub>2</sub>SnS<sub>3</sub> POR EL MÉTODO SILAR PARA SU APLICACIÓN COMO ABSORBEDOR EN CELDAS SOLARES.
- [22] Lokhande CD, Sankapal BR, Pathan HM, Muller M, Giersig M, Tributsch H. Some structural studies on successive ionic layer adsorption and reaction (SILAR)-deposited CdS thin films.
- [23] Kaur I, Pandya DK, Chopra KL. Growth Kinetics and Polymorphism of Chemically Deposited CdS Films. *Journal of The Electrochemical Society*. 1980 Apr 1;127(4):943–8.
- [24] Senthamilselvi V, Saravanakumar K, Anandhi R, Ravichandran AT, Ravichandran K. Effect of annealing on the stoichiometry of CdS films deposited by SILAR technique [Internet]. Vol. 5, *OPTOELECTRONICS AND ADVANCED MATERIALS-RAPID COMMUNICATIONS*. 2011. Available from: <https://www.researchgate.net/publication/279589052>
- [25] Peng XY, Gu HW, Zhang T, Ding FZ, Qu F, Wang HY. Growth mechanism of CdS film prepared by chemical bath deposition. *Rare Metals*. 2014;33(3):324–9.
- [26] Aquí-Romero F, Willars-Rodríguez FJ, Chávez-Urbiola IR, Ramírez-Bon R. ZnO<sub>2</sub> films by successive ionic layer adsorption and reaction method and their conversion to ZnO ones for p-Si/n-ZnO photodiode applications. ZnO<sub>2</sub> films by successive ionic layer adsorption and reaction method and their conversion to ZnO ones for p-Si/n-ZnO photodiode applications. 2019; Available from: <https://doi.org/10.1088/1361->
- [27] Senthamilselvi V, Ravichandran K, Saravanakumar K. Influence of immersion cycles on the stoichiometry of CdS films deposited by SILAR technique. *Journal of Physics and Chemistry of Solids*. 2013 Jan;74(1):65–9.

